Eur. Phys. J. C (2010) 65: 615–635
DOI 10.1140/epjc/s10052-009-1194-9

THE EUROPEAN PHYSICAL JOURNAL C

Regular Article - Theoretical Physics

# Numerical tests of causal relativistic dissipative fluid dynamics

**E. Molnár**[1], **H. Niemi**[1,a], **D.H. Rischke**[1,2]

[1]Frankfurt Institute for Advanced Studies, Ruth-Moufang-Str. 1, 60438 Frankfurt am Main, Germany
[2]Institut für Theoretische Physik, Johann Wolfgang Goethe-Universität, Max-von-Laue-Str. 1, 60438 Frankfurt am Main, Germany

Received: 2 September 2009 / Published online: 21 November 2009


**Abstract** We present numerical methods to solve the Israel–Stewart (IS) equations of causal relativistic dissipative fluid dynamics with bulk and shear viscosities. We then test these methods studying the Riemann problem in $(1+1)$- and $(2+1)$-dimensional geometry. The numerical schemes investigated here are applicable to realistic $(3+1)$-dimensional modeling of a relativistic dissipative fluid.

**PACS** 24.10.Nz · 25.75.-q · 47.11.-j · 47.75.+f

## 1 Introduction

The interest in modeling the evolution of matter created in relativistic heavy-ion collisions with fluid dynamics has never ceased since the pioneering works by Landau [1]. Recent remarkable discoveries at the Relativistic Heavy Ion Collider (RHIC) at Brookhaven National Laboratory provide evidence for an almost "perfect" fluid-like behavior of the QCD matter created [2].

In a perfect, or ideal, fluid, transport coefficients like bulk and shear viscosity and heat conductivity vanish. This is an idealized situation; in a real fluid one can show that there are lower bounds for these transport coefficients, for instance using the uncertainty principle [3] or applying the AdS/CFT conjecture [4]. In order to decide how close to a perfect fluid the matter created at RHIC is, one has perform theoretical calculations in the framework of causal relativistic dissipative fluid dynamics. In this way, one may also be able to extract the numerical values for the bulk and shear viscosity coefficients from experimental measurements.

Currently the most widely accepted and studied theory of relativistic dissipative fluid dynamics is due to Israel and Stewart [5–8]. This is the relativistic version of the pioneering work by Müller [9, 10]. Although these theories have been developed in the 1970s, efforts to study and apply them to relativistic heavy-ion collisions have only started very recently [11, 12]. This has been followed by an impressive number of studies in $(1+1)$-dimensional [13–16] and $(2+1)$-dimensional geometries [17–24].

In $3+1$ dimensions, given arbitrary initial conditions and a general equation of state, the only way to solve the equations of relativistic fluid dynamics is by means of numerical methods. Any numerical method requires an algorithm that has to be tested in order to assess its validity for solving the underlying equations. Testing algorithms to solve relativistic dissipative fluid dynamics is made difficult by the fact that there is only a rather limited number of test cases with analytical solutions. Reference [14] investigated sound propagation for the linearized IS equations. The algorithm of Ref. [21] was checked, for certain expansion scenarios, as to whether it correctly approaches the Navier–Stokes and ideal-fluid limits. So far, however, numerical algorithms to solve the IS equations have not been tested in situations where shock discontinuities occur in the ideal-fluid limit. The present paper, in which we perform an extensive study of the relativistic Riemann problem in $1+1$ and $2+1$ dimensions, aims to fill this gap.

In Sect. 2 we provide a short review of IS theory of dissipative fluid dynamics. In Sect. 3 we formulate it in a form suitable for numerical implementation. This is followed in Sect. 4 by an introductory presentation to the numerical methods which we use to solve the IS equations. In Sect. 5 we report results of solving the Riemann problem in $1+1$ and $2+1$ dimensions. Section 6 concludes this work with a summary of our results and an outlook.

## 2 Dissipative fluid dynamics

### 2.1 Units and definitions

Throughout this work natural units, $\hbar = c = k_B = 1$, are used. Components of contravariant vectors and tensors in

[a] e-mail: niemi@th.physik.uni-frankfurt.de

4-dimensional space-time are denoted by upper indices, i.e., $A^\mu$ and $A^{\mu\nu}$. Greek indices take values from 0 to 3 and Roman indices from 1 to 3. Covariant components, denoted by lower indices, are obtained by $A_\nu \equiv g_{\mu\nu}A^\mu$, where $g_{\mu\nu}$ is the metric tensor, for which we use the $(+,-,-,-)$ convention. If not stated otherwise the Einstein summation convention is used for both Greek and Roman indices.

For an arbitrary contravariant four-vector $A^\mu$ the covariant derivative is defined as

$$A^\mu_{;\alpha} \equiv \partial_\alpha A^\mu + \Gamma^\mu_{\alpha\beta}A^\beta, \tag{1}$$

where $\Gamma^\mu_{\alpha\beta} \equiv \frac{1}{2}g^{\mu\nu}(\partial_\beta g_{\alpha\nu} + \partial_\alpha g_{\nu\beta} - \partial_\nu g_{\alpha\beta})$ denotes the Christoffel symbol of the second kind and $\partial_\alpha = \partial/\partial x^\alpha$ denotes the four-derivative. Similarly, the covariant derivative of covariant vectors is given by $A_{\mu;\alpha} \equiv \partial_\alpha A_\mu - \Gamma^\beta_{\mu\alpha}A_\beta$. For scalars the covariant derivative reduces to the ordinary four-derivative. The covariant derivative of second-rank contravariant tensors is

$$A^{\mu\nu}_{;\alpha} \equiv \partial_\alpha A^{\mu\nu} + \Gamma^\mu_{\alpha\beta}A^{\beta\nu} + \Gamma^\nu_{\alpha\beta}A^{\mu\beta}. \tag{2}$$

Vectors and tensors can be decomposed into parts parallel and orthogonal to the four-velocity of matter $u^\mu$, where $u^\mu u_\mu = 1$. Using the transverse projection operator $\Delta^{\mu\nu} \equiv g^{\mu\nu} - u^\mu u^\nu$ where $\Delta^{\mu\nu}u_\nu = 0$, an arbitrary four-vector can be written as $A^\mu = u^\mu u_\alpha A^\alpha + \Delta^{\mu\alpha}A_\alpha$. The covariant derivative of an arbitrary tensor can be decomposed as

$$A^{\mu_1\cdots\mu_n}_{;\alpha} \equiv u_\alpha DA^{\mu_1\cdots\mu_n} + \nabla_\alpha A^{\mu_1\cdots\mu_n}, \tag{3}$$

where the convective time derivative $D$ and the spatial gradient operator $\nabla_\alpha$ are given by

$$DA^{\mu_1\cdots\mu_n} \equiv u^\beta A^{\mu_1\cdots\mu_n}_{;\beta}, \tag{4}$$

$$\nabla_\alpha A^{\mu_1\cdots\mu_n} \equiv \Delta^\beta_\alpha A^{\mu_1\cdots\mu_n}_{;\beta}. \tag{5}$$

It is convenient to define the traceless and symmetric projection of a tensor field, which is orthogonal to $u^\mu$. This is denoted by angular brackets $\langle\rangle$,

$$A^{\langle\mu\nu\rangle} \equiv \frac{1}{2}\Delta^{\mu\alpha}\Delta^{\nu\beta}(A_{\alpha\beta} + A_{\beta\alpha}) - \frac{1}{3}\Delta^{\mu\nu}\Delta_{\alpha\beta}A^{\alpha\beta}. \tag{6}$$

The covariant derivative of the four-velocity can be generally decomposed as

$$u_{\nu;\mu} = u_\mu Du_\nu + \sigma_{\mu\nu} + \frac{1}{3}\Delta_{\mu\nu}\theta - \omega_{\mu\nu}, \tag{7}$$

where the expansion rate $\theta$, the shear tensor $\sigma_{\mu\nu}$, and the vorticity tensor $\omega_{\mu\nu}$ are defined as

$$\theta \equiv \nabla_\mu u^\mu = \partial_\mu u^\mu + \Gamma^\mu_{\alpha\mu}u^\alpha, \tag{8}$$

$$\begin{aligned}\sigma^{\mu\nu} &\equiv \nabla^{\langle\mu}u^{\nu\rangle} = \frac{1}{2}\Delta^{\mu\alpha}\Delta^{\nu\beta}(u_{\alpha;\beta} + u_{\beta;\alpha}) - \frac{\theta}{3}\Delta^{\mu\nu} \\ &= \frac{1}{2}\big(\partial^\mu u^\nu - u^\mu u^\alpha\partial_\alpha u^\nu + \partial^\nu u^\mu - u^\nu u^\alpha\partial_\alpha u^\mu\big) \\ &\quad + \frac{1}{2}\big(\Delta^{\mu\alpha}u^\beta\Gamma^\nu_{\alpha\beta} + \Delta^{\nu\alpha}u^\beta\Gamma^\mu_{\alpha\beta}\big) - \frac{\theta}{3}\Delta^{\mu\nu},\end{aligned} \tag{9}$$

$$\begin{aligned}\omega^\mu_{\ \nu} &\equiv \frac{1}{2}\Delta^{\mu\alpha}\Delta^\beta_\nu(u_{\alpha;\beta} - u_{\beta;\alpha}) \\ &= \frac{1}{2}\big(\partial_\nu u^\mu - \partial^\mu u_\nu + u^\mu u^\alpha\partial_\alpha u_\nu - u_\nu u^\alpha\partial_\alpha u^\mu\big),\end{aligned} \tag{10}$$

where $\sigma^{\mu\nu}u_\nu = 0$ and $\omega^{\mu\nu}u_\nu = 0$.

### 2.2 The equations of causal relativistic dissipative fluid dynamics

The basic quantities characterizing dissipative fluids are the net charge current $N^\mu$ and the energy–momentum tensor $T^{\mu\nu}$. Following Refs. [25–28] these can be decomposed with respect to the fluid four-velocity $u^\mu$ as

$$N^\mu \equiv N^\mu_{\rm eq} + \delta N^\mu = nu^\mu + V^\mu, \tag{11}$$

$$\begin{aligned}T^{\mu\nu} &\equiv T^{\mu\nu}_{\rm eq} + \delta T^{\mu\nu} = eu^\mu u^\nu - (p + \Pi)\Delta^{\mu\nu} \\ &\quad + W^\mu u^\nu + W^\nu u^\mu + \pi^{\mu\nu},\end{aligned} \tag{12}$$

where $n \equiv N^\mu u_\mu$ is the net charge density and $e \equiv u_\mu T^{\mu\nu}u_\nu$ is the energy density in the local rest frame (LRF), i.e., where $u^\mu = (1,0,0,0)$. The charge diffusion current is given by $\delta N^\mu \equiv V^\mu = N_\nu\Delta^{\mu\nu}$. The energy–momentum flow orthogonal to $u^\mu$ is given by $W^\mu \equiv \Delta^{\mu\alpha}T_{\alpha\beta}u^\beta$. This quantity can be decomposed as $W^\mu \equiv q^\mu + (e+p)V^\mu/n$, where $q^\mu$ is the heat flow. The local isotropic pressure is denoted by $p + \Pi \equiv -\frac{1}{3}\Delta_{\mu\nu}T^{\mu\nu}$, where $p$ is the equilibrium pressure and $\Pi$ is the bulk viscous pressure measuring the deviation from the local equilibrium pressure. The shear stress tensor is defined as $\pi^{\mu\nu} \equiv T^{\langle\mu\nu\rangle}$. This representation is completely general, valid in any coordinate system, and independent of the definition of the flow velocity.

Usually, there are two typical choices used to define the flow velocity: either tied to the net charge flow when $V^\mu = 0$ (Eckart frame) or tied to the energy flow when $W^\mu = 0$ (Landau frame). We will use the latter definition in this work.

Without conserved charges only Landau's definition of the flow velocity is appropriate. In this case the heat flow is $q^\mu = -(e+p)V^\mu/n$. For net charge-free matter, $q^\mu$ is not well defined, but also irrelevant for the discussion, so we set it to zero, $q^\mu = V^\mu = 0$.

When all dissipative quantities are zero, $V^\mu = W^\mu = \Pi = \pi^{\mu\nu} = 0$, the decompositions (11) and (12) reduce to perfect-fluid form, $N^\mu = N^\mu_{\rm eq} \equiv nu^\mu$ and $T^{\mu\nu} = T^{\mu\nu}_{\rm eq} \equiv eu^\mu u^\nu - p(e,n)\Delta^{\mu\nu}$. The LRF energy and charge densities

are always fixed to their equilibrium values by the Landau matching conditions, i.e., $n = n_{\rm eq}$, and $e = e_{\rm eq}$. Then, the equilibrium pressure is given by the equation of state (EOS) $p = p(e,n) \equiv -\frac{1}{3}\Delta_{\mu\nu}T^{\mu\nu}_{\rm eq}$.

The equations of relativistic dissipative fluid dynamics follow from the covariant differentiation of the conserved charge four-current and the energy–momentum tensor,

$$N^{\mu}_{;\mu} \equiv \frac{1}{\sqrt{g}}\,\partial_\mu\big(\sqrt{g}\,N^\mu\big) = 0, \tag{13}$$

$$T^{\mu\nu}_{;\mu} \equiv \frac{1}{\sqrt{g}}\,\partial_\mu\big(\sqrt{g}\,T^{\mu\nu}\big) + \Gamma^{\nu}_{\mu\beta}T^{\mu\beta} = 0, \tag{14}$$

where $g \equiv -\det(g_{\mu\nu})$ is the negative determinant of the metric tensor.

The non-equilibrium entropy current can be written as

$$S^\mu \equiv S^\mu_{\rm eq} + \delta S^\mu = su^\mu + \Phi^\mu, \tag{15}$$

where the entropy flux relative to $u^\mu$ is $\Phi^\mu = S_\nu\Delta^{\mu\nu}$. The LRF entropy density is $s = S^\mu u_\mu$, where in general $s \le s_{\rm eq}(e,n)$.

Following Refs. [5–8], the phenomenological extension of the entropy four-current by Israel and Stewart can be written without heat conductivity as

$$S^\mu \equiv su^\mu = s_{\rm eq}u^\mu - \big(\beta_0\Pi^2 + \beta_2\pi^{\alpha\beta}\pi_{\alpha\beta}\big)\frac{u^\mu}{2T}, \tag{16}$$

where the coefficients $\beta_0, \beta_2$ are functions of $e$ and $n$. Their exact value can be determined explicitly e.g. from kinetic theory.

The requirement of non-decreasing entropy leads to relaxation equations for the bulk pressure and shear stress tensor. Here we also include the vorticity terms which follow from the kinetic-theory derivation, but we neglect the coupling between bulk and shear viscosity. Then, the IS equations [8, 16] read

$$D\Pi = \frac{1}{\tau_\Pi}(\Pi_{\rm NS} - \Pi) - I_0, \tag{17}$$

$$D\pi^{\mu\nu} = \frac{1}{\tau_\pi}\big(\pi^{\mu\nu}_{\rm NS} - \pi^{\mu\nu}\big) - I_1^{\mu\nu} - I_2^{\mu\nu} - I_3^{\mu\nu}, \tag{18}$$

where $\tau_\Pi = \zeta\beta_0$ denotes the relaxation time of the bulk viscous pressure and $\tau_\pi = 2\eta\beta_2$ is the relaxation time of the shear stress tensor. The relativistic Navier–Stokes values are given by [25, 26]

$$\Pi_{\rm NS} \equiv -\zeta\theta, \tag{19}$$

$$\pi^{\mu\nu}_{\rm NS} \equiv 2\eta\sigma^{\mu\nu}, \tag{20}$$

where $\zeta \ge 0$ is the bulk viscosity coefficient and $\eta \ge 0$ is the shear viscosity coefficient. In (17), (18), we introduced the abbreviations

$$I_0 \equiv \frac{1}{2}\Pi\left(\nabla_\lambda u^\lambda + D\ln\frac{\beta_0}{T}\right), \tag{21}$$

$$I_1^{\mu\nu} \equiv \big(\pi^{\lambda\mu}u^\nu + \pi^{\lambda\nu}u^\mu\big)Du_\lambda, \tag{22}$$

$$I_2^{\mu\nu} \equiv \frac{1}{2}\pi^{\mu\nu}\left(\nabla_\lambda u^\lambda + D\ln\frac{\beta_2}{T}\right), \tag{23}$$

$$I_3^{\mu\nu} \equiv 2\pi^{\langle\mu}_\lambda\omega^{\nu\rangle\lambda} = \pi^{\mu\lambda}\omega^\nu{}_\lambda + \pi^{\nu\lambda}\omega^\mu{}_\lambda, \tag{24}$$

where we used $\pi^{\mu\nu}\omega_{\mu\nu} = 0$.

For the sake of simplicity, in our numerical studies presented in the subsequent sections we assume a gas of massless Boltzmann particles without conserved charges. In this case, the equation of state is simply $e = 3p$ and $e = \frac{3g}{\pi^2}T^4$, where $g$ is the number of degrees of freedom. The equilibrium entropy density is given by $s_{\rm eq} = \frac{4g}{\pi^2}T^3$. In this case, we can further simplify $I_2^{\mu\nu}$ noting that the exact value of the thermodynamic integral for massless Boltzmann gas is, $\beta_2 = 3/(4p)$ [8, 30]. Therefore, it follows that $D\beta_2/\beta_2 = -De/e$. Thus, $D\ln(\beta_2/T) = -De/e - DT/T$, where the temperature can be calculated from the EOS. The convective time derivative of the LRF energy density is given by energy conservation, $De = -(e+P)u^\mu_{;\mu} - \pi^{\mu\nu}u_{\mu;\nu}$, where the effective pressure $P$ is defined as $P(e,n,\Pi) = p(e,n) + \Pi$.

### 2.3 General coordinate representation

Here we give the relations between $T^{\mu\nu}$ and $N^\mu$ in the calculational, or laboratory, frame and the LRF densities $e$, $n$, and the flow velocity $v^i$. The natural frame of reference is the laboratory frame. However, during the time evolution of the system, we have to extract the local velocity and the LRF densities from the laboratory frame quantities. These are needed because the EOS is given as a function of LRF densities, $p = p(e,n)$.

We can write the four-vector and tensor quantities given in (11), (12) by specifying the four-velocity of the matter, $u^\mu = \gamma(1, v_i) = \gamma(1, v_x, v_y, v_z)$, where $\gamma = (1-v^2)^{-1/2}$ and $v \equiv |\mathbf{v}| = (v_x^2 + v_y^2 + v_z^2)^{1/2}$. The laboratory frame quantities take the form

$$N^0 \equiv n\gamma, \tag{25}$$

$$N^i \equiv n\gamma v_i = v_i N^0, \tag{26}$$

$$T^{00} \equiv (e+P)\gamma^2 - g^{00}P + \pi^{00}, \tag{27}$$

$$\begin{aligned} T^{0i} &\equiv (e+P)\gamma^2 v_i - g^{0i}P + \pi^{0i} \\ &= v_i T^{00} + P\big(g^{00}v_i - g^{0i}\big) - v_i\pi^{00} + \pi^{0i}, \end{aligned} \tag{28}$$

$$\begin{aligned} T^{ij} &\equiv (e+P)\gamma^2 v_i v_j - Pg^{ij} + \pi^{ij} \\ &= v_i T^{0j} + P\big(g^{0j}v_i - g^{ij}\big) - v_i\pi^{0j} + \pi^{ij}. \end{aligned} \tag{29}$$

$N^0$ is the local charge density, $N^i$ is the local charge current in the direction $i$, i.e., the direction of the flow $u^i$. The total energy density of the fluid is $T^{00}$ which in the LRF reduces to the (equilibrium) energy density $e$. By definition, $T^{0i}$ denotes the energy flow in the direction of $u^i$, while $T^{i0}$ is the momentum density flux in the $i$th direction.[1] The remaining spatial part, $T^{ij}$, denotes the $i$th component of the momentum flowing in direction $j$.

The LRF charge density and energy density are obtained from (25) and (27), (28), respectively,

$$n = N^0\big(1-v^2\big)^{1/2}, \tag{30}$$

$$e = T^{00} - \pi^{00} - v_i\big(T^{0i} - \pi^{0i}\big), \tag{31}$$

while (28) together with the above expressions leads to the expression for the velocity components,

$$v_i = \frac{T^{0i} - \pi^{0i} + Pg^{0i}}{T^{00} - \pi^{00} + Pg^{00}}. \tag{32}$$

In most cases of interest $g^{00} = 1$, and the metric of the space-time is diagonal. Therefore we can introduce a simplified notation which mimics the perfect-fluid relations [29], $R = n\gamma$, $E \equiv T^{00} - \pi^{00}$, $M_i \equiv T^{0i} - \pi^{0i}$, where $M \equiv |\mathbf{M}| = (M_x^2 + M_y^2 + M_z^2)^{1/2}$. Thus, $\mathbf{M}$ is parallel to the velocity $\mathbf{v}$, similarly as in the perfect-fluid case. These quantities have to obey the physical constraint $M \le E$, in order to obtain meaningful solutions. Therefore, we can express the LRF charge density, energy density, the absolute magnitude of the velocity, and the velocity components as

$$n = R(1 - \mathbf{v}\cdot\mathbf{v})^{1/2}, \tag{33}$$

$$e = E - \mathbf{v}\cdot\mathbf{M}, \tag{34}$$

$$v = M/[E+P], \tag{35}$$

$$v_i = vM_i/M. \tag{36}$$

Substituting (33), (34) into (35) we obtain the equation for the magnitude of the velocity, $v$. This can be solved by using a one-dimensional root search. Thereafter, use of (36) yields the individual velocity components and $\gamma$. Note that, in the case of perfect fluids, this simplified treatment is practicable, however, in case of dissipative fluids, this may not always be possible. This is due to the fact that the vectors $T^{0\mu}$ and $\pi^{0\mu}$ are not parallel to each other. Hence choosing other shear stress tensor components as independent variables, or in cases which take into account the heat flow, it is required to carry out a multidimensional root search to find the velocity [18, 22, 29, 31].

[1] In standard units the flow of the energy density is $cT^{0i}$, while the flow of momentum density is $c^{-1}T^{i0}$.

For dissipative fluids the number of unknown variables increases by the introduction of the shear stress tensor and the bulk viscosity. The shear stress tensor is constrained by the orthogonality condition $\pi^{\mu\nu}u_\nu = 0$, leading to the following relations,

$$\pi^{i0}u_0 \equiv -\pi^{ij}u_j, \tag{37}$$

$$\pi^{00}u_0 \equiv -\pi^{0i}u_i = \pi^{ij}u_ju_i/u_0. \tag{38}$$

One more independent relation follows from the trace of the shear stress tensor, $\pi^\mu_\mu = 0$,

$$\pi^{00} \equiv -\pi^{ii}g_{ii}. \tag{39}$$

In general, using (37) we can reduce the number of unknowns by three, and by two using (38) and (39). Thus we are left with five independent components of the shear stress tensor. However, for testing the numerical solutions it is preferable to calculate all shear stress tensor components directly using the relaxation equations, instead of using the orthogonality relations. We will return to this matter later and provide examples.

## 3 Test problems

In this section we shall write the IS equations in various $(1+1)$- and $(2+1)$-dimensional geometries with Cartesian or curvilinear coordinates. For the sake of completeness, the $(2+1)$-dimensional boost-invariant and the $(3+1)$-dimensional IS equations in Cartesian as well as in $(\tau, x, y, \eta)$ coordinates are given in the appendices. Here $\tau$ is the longitudinal proper time and $\eta$ is the space-time rapidity.

### 3.1 $(1+1)$-dimensional Cartesian coordinates

In Cartesian coordinates, the metric tensor is $g^{\mu\nu} \equiv \eta^{\mu\nu} = \mathrm{diag}(1,-1,-1,-1)$ and all Christoffel symbols vanish. The negative determinant of the metric is $g = 1$. We assume that the system evolves along the $z$ direction and that it is homogeneous in the transverse plane, such that the spatial derivatives in $x$ and $y$ directions vanish identically. The flow velocity of matter is $u^\mu = \gamma_z(1,0,0,v_z)$ and $\gamma_z = (1-v_z^2)^{-1/2}$.

The components of the energy–momentum tensor and charge current in the laboratory frame are

$$N^0 \equiv n\gamma_z, \tag{40}$$

$$N^z \equiv N^0 v_z, \tag{41}$$

$$T^{00} \equiv (e+P)\gamma_z^2 - P + \pi^{00} = (e+P_z)\gamma_z^2 - P_z, \tag{42}$$

$$T^{0z} \equiv (e+P)\gamma_z^2 v_z + \pi^{0z} = (e+P_z)\gamma_z^2 v_z, \tag{43}$$

$$T^{xx} \equiv \pi^{xx} + P = -\frac{\pi}{2} + P, \tag{44}$$

$$T^{yy} \equiv \pi^{yy} + P = -\frac{\pi}{2} + P, \tag{45}$$

$$T^{zz} \equiv (e+P)\gamma_z^2 v_z^2 + P + \pi^{zz} = \left(ev_z^2 + P_z\right)\gamma_z^2, \tag{46}$$

where the shear pressure, $\pi$, is defined such that $\pi^{zz} = \gamma_z^2 \pi$. The orthogonality and tracelessness properties imply $\pi^{xx} = \pi^{yy} = -\pi/2$, and $\pi^{00} = v_z^2 \gamma_z^2 \pi$, see Ref. [31]. From the orthogonality relation we obtain $\pi^{0z} = v_z \pi^{zz} = v_z \gamma_z^2 \pi$. The effective pressure in the $z$ direction is denoted by $P_z \equiv P + \pi = p(e,n) + \Pi + \pi$. The remaining four-vector and tensor components vanish, $N^x = N^y = 0$ and $T^{0x} = T^{0y} = T^{xy} = T^{xz} = T^{yz} = 0$. This also means that the corresponding shear stress tensor components vanish, $\pi^{0x} = \pi^{0y} = \pi^{xy} = \pi^{xz} = \pi^{yz} = 0$.

The LRF quantities and the velocity can be expressed in terms of the laboratory quantities,

$$n = N^0\left(1 - v_z^2\right)^{1/2}, \tag{47}$$

$$e = T^{00} - v_z T^{0z}, \tag{48}$$

$$v_z = \frac{T^{0z}}{T^{00} + P_z}. \tag{49}$$

The conservation equations follow from (13), (14),

$$\partial_t N^0 + \partial_z\left(v_z N^0\right) = 0, \tag{50}$$

$$\partial_t T^{00} + \partial_z\left(v_z T^{00}\right) = -\partial_z(v_z P_z), \tag{51}$$

$$\partial_t T^{0z} + \partial_z\left(v_z T^{0z}\right) = -\partial_z P_z. \tag{52}$$

The relaxation equations for the bulk viscous and shear pressure follow from (17), (18):

$$\gamma_z \partial_t \Pi + \gamma_z v_z \partial_z \Pi = \frac{1}{\tau_\Pi}(\Pi_{\mathrm{NS}} - \Pi) - I_0, \tag{53}$$

$$\gamma_z \partial_t \pi + \gamma_z v_z \partial_z \pi = \frac{1}{\tau_\pi}(\pi_{\mathrm{NS}} - \pi) - I_2, \tag{54}$$

where $I_1^{xx} = I_3^{xx} = 0$. The Navier–Stokes values of the bulk viscous and shear pressure are

$$\Pi_{\mathrm{NS}} \equiv -\zeta\theta_z, \tag{55}$$

$$\pi_{\mathrm{NS}} \equiv 2\eta\sigma = -\frac{4}{3}\eta\theta_z, \tag{56}$$

where $\theta_z \equiv \partial_\mu u^\mu = \partial_t \gamma_z + \partial_z(\gamma_z v_z) = \nabla_\mu u^\mu$ denotes the expansion scalar and $\sigma = -2\sigma^{xx} = \theta_z/3$ is the shear stress. Furthermore (21) and (23) with $I_2 = -2I_2^{xx}$, lead to

$$I_0 = \frac{\Pi}{2}\left(\theta_z + D\ln\frac{\beta_0}{T}\right), \tag{57}$$

$$I_2 = \frac{\pi}{2}\left(\theta_z + D\ln\frac{\beta_2}{T}\right). \tag{58}$$

### 3.2 (1 + 1)-dimensional cylindrical coordinates

In the case of (1 + 1)-dimensional cylindrical coordinates, all quantities are functions of the time $t$ and the radial coordinate $r$ only. The flow velocity is given by $u^\mu = \gamma_r(1, v_r, 0, 0)$, where $\gamma_r = (1 - v_r^2)^{-1/2}$. The gradient operator is $\partial_\mu = (\partial_t, \partial_r, 0, 0)$. The terms containing $\partial_\phi$ and $\partial_z$ vanish identically.

The metric tensor transforms as $g_{\mu\nu} = \frac{\partial \tilde{x}^\alpha}{\partial x^\mu}\frac{\partial \tilde{x}^\beta}{\partial x^\nu}\eta_{\alpha\beta}$, where $x^\mu = (t, r, \phi, z)$, $\tilde{x}^\mu = (t, x, y, z)$ and $\eta_{\mu\nu}$ is the Cartesian metric. The spatial coordinates are $r = \sqrt{x^2 + y^2}$ and $\phi = \arctan(y/x)$. The contravariant and covariant metric tensors are $g^{\mu\nu} = \mathrm{diag}(1, -1, -1/r^2, -1)$ and $g_{\mu\nu} = \mathrm{diag}(1, -1, -r^2, -1)$, respectively. The negative determinant is $g = r^2$. The only non-vanishing Christoffel symbols are $\Gamma^\phi_{\phi r} = \Gamma^\phi_{r\phi} = r^{-1}$ and $\Gamma^r_{\phi\phi} = -r$.

The laboratory frame quantities are

$$N^0 \equiv n\gamma_r, \tag{59}$$

$$N^r \equiv N^0 v_r, \tag{60}$$

$$T^{00} \equiv (e+P)\gamma_r^2 - P + \pi^{00} = (e+P_r)\gamma_r^2 - P_r, \tag{61}$$

$$T^{0r} \equiv (e+P)\gamma_r^2 v_r + \pi^{0r} = (e+P_r)\gamma_r^2 v_r, \tag{62}$$

$$T^{rr} \equiv (e+P)\gamma_r^2 v_r^2 + P + \pi^{rr} = (e+P_r)\gamma_r^2 v_r^2 + P_r, \tag{63}$$

$$T^{\phi\phi} \equiv \frac{P}{r^2} + \pi^{\phi\phi}, \tag{64}$$

$$T^{zz} \equiv P + \pi^{zz}, \tag{65}$$

where $P_r$ is the effective pressure in the radial direction defined below. All remaining vector and tensor components vanish identically, $N^\phi = N^z = 0$, $T^{0\phi} = T^{0z} = T^{\phi r} = T^{\phi z} = T^{rz} = 0$ and $\pi^{0\phi} = \pi^{0z} = \pi^{\phi r} = \pi^{\phi z} = \pi^{rz} = 0$.

To reduce the number of unknowns we use the transversality of the shear stress tensor, leading to $\pi^{0r} = v_r \pi^{rr}$, $\pi^{00} = v_r^2 \pi^{rr}$. The tracelessness condition gives $\pi^{00} = \pi^{rr} + r^2\pi^{\phi\phi} + \pi^{zz}$. The simplest solution is to choose $\pi^{\phi\phi}$ and $\pi^{zz}$ as the independent components of the shear stress tensor, since a Lorentz boost in radial direction does not affect these components. The remaining shear stress tensor components can be expressed by using these components,

$$\pi^{rr} = -\gamma_r^2\left(r^2\pi^{\phi\phi} + \pi^{zz}\right), \tag{66}$$

$$\pi^{0r} = -v_r\gamma_r^2\left(r^2\pi^{\phi\phi} + \pi^{zz}\right), \tag{67}$$

$$\pi^{00} = -v_r^2\gamma_r^2\left(r^2\pi^{\phi\phi} + \pi^{zz}\right). \tag{68}$$

The LRF charge density, energy density, and velocity are given as

$$n = N^0\left(1 - v_r^2\right)^{1/2}, \tag{69}$$

$$e = T^{00} - v_r T^{0r}, \tag{70}$$

$$v_r = \frac{T^{0r}}{T^{00} + P_r}, \tag{71}$$

where $P_r \equiv P + \frac{\pi^{rr}}{\gamma_r^2} = P - r^2\pi^{\phi\phi} - \pi^{zz}$.

The charge conservation equation and the equations of energy and momentum conservation follow from (13), (14),

$$\partial_t N^0 + \partial_r\left(v_r N^0\right) = -\frac{1}{r}\left(v_r N^0\right), \tag{72}$$

$$\begin{aligned}\partial_t T^{00} + \partial_r\left(v_r T^{00}\right) = &-\partial_r\left(v_r P_r\right)\\ &-\frac{1}{r}\left(v_r T^{00} + v_r P_r\right),\end{aligned} \tag{73}$$

$$\begin{aligned}\partial_t T^{0r} + \partial_r\left(v_r T^{0r}\right) = &-\partial_r P_r\\ &-\frac{1}{r}\left(v_r T^{0r} - 2r^2\pi^{\phi\phi} - \pi^{zz}\right).\end{aligned} \tag{74}$$

Due to symmetry the right-hand side of (74) has to vanish at the origin. The relaxation equations follow from (17), (18),

$$\gamma_r\partial_t\Pi + \gamma_r v_r\partial_r\Pi = \frac{1}{\tau_\pi}\left(\Pi_{\rm NS} - \Pi\right) - I_0, \tag{75}$$

$$\begin{aligned}\gamma_r\partial_t\pi^{\phi\phi} + \gamma_r v_r\partial_r\pi^{\phi\phi} = &\frac{1}{\tau_\pi}\left(\pi^{\phi\phi}_{\rm NS} - \pi^{\phi\phi}\right)\\ &-2\frac{\gamma_r v_r}{r}\pi^{\phi\phi} - I_2^{\phi\phi},\end{aligned} \tag{76}$$

$$\gamma_r\partial_t\pi^{zz} + \gamma_r v_r\partial_r\pi^{zz} = \frac{1}{\tau_\pi}\left(\pi^{zz}_{\rm NS} - \pi^{zz}\right) - I_2^{zz}, \tag{77}$$

where the expansion scalar is $\theta_r = \partial_t\gamma_r + r^{-1}\partial_r(r\gamma_r v_r)$ and $I_1^{\phi\phi} = I_1^{zz} = I_3^{\phi\phi} = I_3^{zz} = 0$. Note that the convective time derivative from (4) leads to an extra term for the $\pi^{\phi\phi}$ component, which was missed in (5.16) of Ref. [29].

The shear stress tensor components are calculated from (9), hence the Navier–Stokes values for the bulk viscous pressure and shear stress tensor are,

$$\Pi_{\rm NS} \equiv -\zeta\theta_r, \tag{78}$$

$$\pi^{\phi\phi}_{\rm NS} \equiv 2\eta\sigma^{\phi\phi} = \frac{2\eta}{r^2}\left(\frac{\theta_r}{3} - \frac{\gamma_r v_r}{r}\right), \tag{79}$$

$$\pi^{zz}_{\rm NS} \equiv 2\eta\sigma^{zz} = 2\eta\frac{\theta_r}{3}. \tag{80}$$

Also note that the $r^{-2}$ factor in $\pi^{\phi\phi}_{\rm NS}$ might cause problems close to the origin. Hence it is preferable to rewrite the relaxation equation using the following variable: $\tilde\pi^{\phi\phi} = r^2\pi^{\phi\phi}$.

The term $I_0$ and the relevant components of $I_2^{\mu\nu}$ are given by

$$I_0 = \frac{1}{2}\Pi\left(\theta_r + D\ln\frac{\beta_0}{T}\right), \tag{81}$$

$$I_2^{\phi\phi} = \frac{1}{2}\pi^{\phi\phi}\left(\theta_r + D\ln\frac{\beta_2}{T}\right), \tag{82}$$

$$I_2^{zz} = \frac{1}{2}\pi^{zz}\left(\theta_r + D\ln\frac{\beta_2}{T}\right). \tag{83}$$

We also have the following relations between the cylindrically symmetric and Cartesian systems (with similar relations between the shear stress tensor components)

$$T^{0x} = T^{0r}\cos\phi, \tag{84}$$

$$T^{0y} = T^{0r}\sin\phi, \tag{85}$$

$$T^{xx} = T^{rr}\cos^2\phi + r^2T^{\phi\phi}\sin^2\phi, \tag{86}$$

$$T^{yy} = T^{rr}\sin^2\phi + r^2T^{\phi\phi}\cos^2\phi, \tag{87}$$

$$T^{xy} = \left(T^{rr} - r^2T^{\phi\phi}\right)\cos\phi\sin\phi, \tag{88}$$

while $T^{00}$ and $T^{zz}$ remain unchanged. The inverse transformations are

$$T^{0r} = T^{0x}\cos\phi + T^{0y}\sin\phi, \tag{89}$$

$$T^{0\phi} = \left(T^{0y}\cos\phi - T^{0x}\sin\phi\right)/r, \tag{90}$$

$$T^{rr} = T^{xx}\cos^2\phi + T^{xy}\sin(2\phi) + T^{yy}\sin^2\phi, \tag{91}$$

$$T^{\phi\phi} = \left[T^{xx}\sin^2\phi - T^{xy}\sin(2\phi) + T^{yy}\cos^2\phi\right]/r^2, \tag{92}$$

$$T^{r\phi} = \left[\left(T^{yy} - T^{xx}\right)\sin\phi\cos\phi + T^{xy}\cos(2\phi)\right]/r. \tag{93}$$

These relations will be used to compare the evolution of cylindrically symmetric and Cartesian systems.

### 3.3 (2 + 1)-dimensional Cartesian coordinates

For (2 + 1)-dimensional Cartesian coordinates, the covariant derivative of any four-vector reduces to the standard four-divergence, since all Christoffel symbols vanish. We assume that the system is homogeneous in the $z$ direction and the velocity, as well as the derivative in this direction, vanish. Hence the four-flow and four-gradient are function of $(t, x, y)$ coordinates alone, thus $u^\mu = \gamma_\perp(1, v_x, v_y, 0)$, $\partial_\mu = (\partial_t, \partial_x, \partial_y, 0)$, where $\gamma_\perp = (1 - v_\perp^2)^{-1/2}$ and $v_\perp = (v_x^2 + v_y^2)^{1/2}$.

The relevant laboratory frame quantities are

$$N^0 \equiv n\gamma_\perp, \tag{94}$$

$$N^x \equiv N^0 v_x, \tag{95}$$

$$N^y \equiv N^0 v_y, \tag{96}$$

$$T^{00} \equiv (e + P)\gamma_\perp^2 - P + \pi^{00}, \tag{97}$$

$$\begin{aligned}T^{0x} &\equiv (e + P)\gamma_\perp^2 v_x + \pi^{0x}\\ &= v_x T^{00} + v_x P - v_x\pi^{00} + \pi^{0x},\end{aligned} \tag{98}$$

$$T^{0y} \equiv (e+P)\gamma_\perp^2 v_y + \pi^{0y} = v_y T^{00} + v_y P - v_y \pi^{00} + \pi^{0y}, \tag{99}$$

$$T^{xx} \equiv (e+P)\gamma_\perp^2 v_x^2 + P + \pi^{xx} = v_x T^{0x} + P - v_x \pi^{0x} + \pi^{xx}, \tag{100}$$

$$T^{yy} \equiv (e+P)\gamma_\perp^2 v_y^2 + P + \pi^{yy} = v_y T^{0y} + P - v_y \pi^{0y} + \pi^{yy}, \tag{101}$$

$$T^{xy} \equiv (e+P)\gamma_\perp^2 v_x v_y + \pi^{xy} = v_x T^{0y} - v_x \pi^{0y} + \pi^{xy} = v_y T^{0x} - v_y \pi^{0x} + \pi^{xy}, \tag{102}$$

$$T^{zz} = P + \pi^{zz}. \tag{103}$$

The remaining $z$-directed four-vector and tensor components vanish, i.e., $N^z = 0$, $T^{0z} = T^{xz} = T^{yz} = 0$ and $\pi^{0z} = \pi^{xz} = \pi^{yz} = 0$. The LRF charge density and energy density are

$$n = N^0\big(1 - v_x^2 - v_y^2\big)^{1/2}, \tag{104}$$

$$e = T^{00} - \pi^{00} - v_x\big(T^{0x} - \pi^{0x}\big) - v_y\big(T^{0y} - \pi^{0y}\big), \tag{105}$$

while the velocity components from (32) lead to

$$v_x = \frac{T^{0x} - \pi^{0x}}{T^{00} - \pi^{00} + P}, \tag{106}$$

$$v_y = \frac{T^{0y} - \pi^{0y}}{T^{00} - \pi^{00} + P}. \tag{107}$$

The velocity components can be calculated from the equations given above using a two-dimensional root search or via a one-dimensional root search using (35), (36).

Since we previously fixed and explicitly used some shear stress tensor components in the velocity calculation, we choose to express the remaining components in terms of the former. The orthogonality relation (37) and the tracelessness relation (39) yield

$$\pi^{0x} = \pi^{xx} v_x + \pi^{xy} v_y, \tag{108}$$

$$\pi^{0y} = \pi^{xy} v_x + \pi^{yy} v_y, \tag{109}$$

$$\pi^{00} = \pi^{xx} + \pi^{yy} + \pi^{zz}. \tag{110}$$

Therefore, as function of the chosen independent variables, $\pi^{00}, \pi^{0x}, \pi^{0y}$, and $\pi^{zz}$, the other shear stress tensor components are

$$\pi^{xx} = \big[v_y^2\big(\pi^{00} - \pi^{zz}\big) + v_x \pi^{0x} - v_y \pi^{0y}\big]/v_\perp^2, \tag{111}$$

$$\pi^{yy} = \big[v_x^2\big(\pi^{00} - \pi^{zz}\big) - v_x \pi^{0x} - v_y \pi^{0y}\big]/v_\perp^2, \tag{112}$$

$$\pi^{xy} = \big[-v_x v_y\big(\pi^{00} - \pi^{zz}\big) + v_y \pi^{0x} + v_x \pi^{0y}\big]/v_\perp^2. \tag{113}$$

One may then check whether the remaining orthogonality relation,

$$\pi^{00} = \pi^{0x} v_x + \pi^{0y} v_y, \tag{114}$$

is fulfilled. The above relations between the shear stress tensor components become unusable in the case that the velocity in the transverse direction approaches zero. Therefore, in our calculations we shall neglect the above simplifications and calculate all shear stress tensor components explicitly.

Note that one can choose to select $\pi^{xx}, \pi^{yy}$, and $\pi^{xy}$ as independent components, therefore $\pi^{00}, \pi^{0x}, \pi^{0y}$, and $\pi^{zz}$ are given by (108)–(110) and (114), see Refs. [18, 22]. However, in this case the velocity iteration is two-dimensional which may become computationally as expensive as solving the additional transport equations.

The conservation of net charge $N^0$, energy $T^{00}$, and the momentum components $T^{0x}$ and $T^{0y}$ are

$$\partial_t N^0 + \partial_x\big(v_x N^0\big) + \partial_y\big(v_y N^0\big) = 0, \tag{115}$$

$$\partial_t T^{00} + \partial_x\big(v_x T^{00}\big) + \partial_y\big(v_y T^{00}\big) = -\partial_x\big(v_x P - v_x \pi^{00} + \pi^{0x}\big) - \partial_y\big(v_y P - v_y \pi^{00} + \pi^{0y}\big), \tag{116}$$

$$\partial_t T^{0x} + \partial_x\big(v_x T^{0x}\big) + \partial_y\big(v_y T^{0x}\big) = -\partial_x\big(P - v_x \pi^{0x} + \pi^{xx}\big) - \partial_y\big(-v_y \pi^{0x} + \pi^{xy}\big), \tag{117}$$

$$\partial_t T^{0y} + \partial_x\big(v_x T^{0y}\big) + \partial_y\big(v_y T^{0y}\big) = -\partial_x\big(-v_x \pi^{0y} + \pi^{xy}\big) - \partial_y\big(P - v_y \pi^{0y} + \pi^{yy}\big). \tag{118}$$

The relaxation equations for the bulk viscous pressure, $\Pi$, and the components $\pi^{00}, \pi^{0x}, \pi^{0y}, \pi^{xx}, \pi^{yy}, \pi^{zz}, \pi^{xy}$ of the shear stress tensor are

$$\gamma_\perp \partial_t \Pi + \gamma_\perp v_x \partial_x \Pi + \gamma_\perp v_y \partial_y \Pi = \frac{1}{\tau_\Pi}(\Pi_{\mathrm{NS}} - \Pi) - I_0, \tag{119}$$

$$\gamma_\perp \partial_t \pi^{\mu\nu} + \gamma_\perp v_x \partial_x \pi^{\mu\nu} + \gamma_\perp v_y \partial_y \pi^{\mu\nu} = \frac{1}{\tau_\pi}\big(\pi_{\mathrm{NS}}^{\mu\nu} - \pi^{\mu\nu}\big) - I_1^{\mu\nu} - I_2^{\mu\nu} - I_3^{\mu\nu}, \tag{120}$$

where the Navier–Stokes values are $\Pi_{\mathrm{NS}} \equiv -\zeta\theta_\perp$ and $\pi_{\mathrm{NS}}^{\mu\nu} \equiv 2\eta\sigma^{\mu\nu}$, and the expansion scalar is $\theta_\perp = \partial_t \gamma_\perp + \partial_x(\gamma_\perp v_x) + \partial_y(\gamma_\perp v_y)$.

The components of the shear tensor can be calculated from (9), which reduces to the following simple form $\sigma^{\mu\nu} \equiv \frac{1}{2}(\partial^\mu u^\nu - u^\mu D u^\nu + \partial^\nu u^\mu - u^\nu D u^\mu) - \frac{\theta_\perp}{3}\Delta^{\mu\nu}$ in Cartesian coordinates. Hence,

$$\sigma^{00} = \partial_t \gamma_\perp - \gamma_\perp D\gamma_\perp + \big(\gamma_\perp^2 - 1\big)\frac{\theta_\perp}{3}, \tag{121}$$

$$\sigma^{0x} = \frac{1}{2}\big[\partial_t(\gamma_\perp v_x) - \partial_x\gamma_\perp\big] - \frac{1}{2}\big[\gamma_\perp D(\gamma_\perp v_x) + \gamma_\perp v_x D\gamma_\perp\big] + \gamma_\perp^2 v_x\frac{\theta_\perp}{3}, \quad (122)$$

$$\sigma^{0y} = \frac{1}{2}\big[\partial_t(\gamma_\perp v_y) - \partial_y\gamma_\perp\big] - \frac{1}{2}\big[\gamma_\perp D(\gamma_\perp v_y) + \gamma_\perp v_y D\gamma_\perp\big] + \gamma_\perp^2 v_y\frac{\theta_\perp}{3}, \quad (123)$$

$$\sigma^{xx} = -\partial_x(\gamma_\perp v_x) - \gamma_\perp v_x D(\gamma_\perp v_x) + \big(1+\gamma_\perp^2 v_x^2\big)\frac{\theta_\perp}{3}, \quad (124)$$

$$\sigma^{yy} = -\partial_y(\gamma_\perp v_y) - \gamma_\perp v_y D(\gamma_\perp v_y) + \big(1+\gamma_\perp^2 v_y^2\big)\frac{\theta_\perp}{3}, \quad (125)$$

$$\sigma^{xy} = -\frac{1}{2}\big[\partial_x(\gamma_\perp v_y) + \partial_y(\gamma_\perp v_x)\big] - \frac{1}{2}\big[\gamma_\perp v_x D(\gamma_\perp v_y) + \gamma_\perp v_y D(\gamma_\perp v_x)\big] + \gamma_\perp^2 v_x v_y\frac{\theta_\perp}{3}, \quad (126)$$

$$\sigma^{zz} = \frac{\theta_\perp}{3}, \quad (127)$$

where $D \equiv u^\mu\partial_\mu = \gamma_\perp\partial_t + \gamma_\perp v_x\partial_x + \gamma_\perp v_y\partial_y$.

The term $I_1^{\mu\nu} = (\pi^{\lambda\mu}u^\nu + \pi^{\lambda\nu}u^\mu)Du_\lambda$ leads to

$$I_1^{00} = 2\gamma_\perp\big[\pi^{00}D\gamma_\perp - \pi^{0x}D(\gamma_\perp v_x) - \pi^{0y}D(\gamma_\perp v_y)\big], \quad (128)$$

$$I_1^{0x} = \gamma_\perp\big[\big(\pi^{00}v_x + \pi^{0x}\big)D\gamma_\perp - \big(\pi^{0x}v_x + \pi^{xx}\big)D(\gamma_\perp v_x) - \big(\pi^{0y}v_x + \pi^{xy}\big)D(\gamma_\perp v_y)\big], \quad (129)$$

$$I_1^{0y} = \gamma_\perp\big[\big(\pi^{00}v_y + \pi^{0y}\big)D\gamma_\perp - \big(\pi^{0x}v_y + \pi^{xy}\big)D(\gamma_\perp v_x) - \big(\pi^{0y}v_y + \pi^{yy}\big)D(\gamma_\perp v_y)\big], \quad (130)$$

$$I_1^{xx} = 2\gamma_\perp v_x\big[\pi^{0x}D\gamma_\perp - \pi^{xx}D(\gamma_\perp v_x) - \pi^{xy}D(\gamma_\perp v_y)\big], \quad (131)$$

$$I_1^{yy} = 2\gamma_\perp v_y\big[\pi^{0y}D\gamma_\perp - \pi^{xy}D(\gamma_\perp v_x) - \pi^{yy}D(\gamma_\perp v_y)\big],$$

$$I_1^{xy} = \gamma_\perp\big[\big(\pi^{0x}v_y + \pi^{0y}v_x\big)D\gamma_\perp - \big(\pi^{xx}v_y + \pi^{xy}v_x\big)D(\gamma_\perp v_x) - \big(\pi^{xy}v_y + \pi^{yy}v_x\big)D(\gamma_\perp v_y)\big], \quad (132)$$

$$(133)$$

and $I_1^{zz} = 0$. The terms $I_0$ and $I_2^{\mu\nu}$ are again given by (21) and (23), respectively. Finally, the components of the term $I_3^{\mu\nu} = \pi^{\mu\lambda}\omega^\nu{}_\lambda + \pi^{\nu\lambda}\omega^\mu{}_\lambda$ are explicitly given by

$$I_3^{00} = 2\big(\pi^{0x}\omega^0{}_x + \pi^{0y}\omega^0{}_y\big), \quad (134)$$

$$I_3^{0x} = \pi^{00}\omega^x{}_0 + \pi^{0y}\omega^x{}_y + \pi^{xx}\omega^0{}_x + \pi^{xy}\omega^0{}_y, \quad (135)$$

$$I_3^{0y} = \pi^{00}\omega^y{}_0 + \pi^{0x}\omega^y{}_x + \pi^{xy}\omega^0{}_x + \pi^{yy}\omega^0{}_y, \quad (136)$$

$$I_3^{xx} = 2\big(\pi^{0x}\omega^x{}_0 + \pi^{xy}\omega^x{}_y\big), \quad (137)$$

$$I_3^{yy} = 2\big(\pi^{0y}\omega^y{}_0 + \pi^{xy}\omega^y{}_x\big), \quad (138)$$

$$I_3^{xy} = \pi^{0x}\omega^y{}_0 + \pi^{xx}\omega^y{}_x + \pi^{0y}\omega^x{}_0 + \pi^{yy}\omega^x{}_y, \quad (139)$$

and $I_3^{zz} = 0$. The vorticity tensor in Cartesian coordinates is given by, $\omega^\mu_\nu \equiv \frac{1}{2}(\partial_\nu u^\mu - \partial^\mu u_\nu + u^\mu Du_\nu - u_\nu Du^\mu)$, therefore the non-vanishing vorticity tensor components are

$$\omega^0{}_x = \frac{1}{2}\big[\partial_x\gamma_\perp + \partial_t(\gamma_\perp v_x)\big] + \frac{1}{2}\big[\gamma_\perp v_x D\gamma_\perp - \gamma_\perp D(\gamma_\perp v_x)\big], \quad (140)$$

$$\omega^0{}_y = \frac{1}{2}\big[\partial_y\gamma_\perp + \partial_t(\gamma_\perp v_y)\big] + \frac{1}{2}\big[\gamma_\perp v_y D\gamma_\perp - \gamma_\perp D(\gamma_\perp v_y)\big], \quad (141)$$

$$\omega^x{}_y = \frac{1}{2}\big[\partial_y(\gamma_\perp v_x) - \partial_x(\gamma_\perp v_y)\big] + \frac{1}{2}\big[\gamma_\perp v_y D(\gamma_\perp v_x) - \gamma_\perp v_x D(\gamma_\perp v_y)\big], \quad (142)$$

where the vorticity tensor components satisfy the following relations, $\omega^0{}_x = \omega^x{}_0 = -\omega^{0x} = \omega_{0x}$, $\omega^0{}_y = \omega^y{}_0 = -\omega^{0y} = \omega_{0y}$ and $\omega^x{}_y = -\omega^y{}_x = -\omega^{xy} = -\omega_{xy}$.

## 4 Numerical methods

In this section we present in detail the numerical algorithm used to solve the equations of relativistic dissipative fluid dynamics in $(1+1)$- and $(2+1)$-dimensional geometries. In our case, this will be the SHArp and Smooth Transport Algorithm (SHASTA) [33]. We also briefly discuss other schemes, and conclude with remarks on the numerical resolution and dissipative fluxes.

### 4.1 One-dimensional implementation

In $(1+1)$-dimensional systems the equations of charge and energy–momentum conservation, (50), (51), (52), are of conservation type and can be generally written as

$$\partial_t U + \partial_x(v_x U) = S(t,x), \quad (143)$$

where $U = U(t,x)$ is the conserved quantity, $v_x$ is the flow velocity in $x$ direction, and $S(t,x)$ is the source term. The

relaxation equations (53), (54) are of convective type. These equations can be rearranged in conservation form with an additional source term [31, 32],

$$\partial_t U_\pi + \partial_x (v_x U_\pi) = U_\pi \partial_x v_x + S_\pi(t,x), \tag{144}$$

where $U_\pi$ is $\Pi$ or $\pi$, and $S_\pi$ is the source term either from (53) or (54) divided by $\gamma = (1 - v_x^2)^{-1/2}$.

To solve the above type of equations numerically, the original partial differential equations are replaced by approximate algebraic difference equations and the values of $U$, $v$, and $S$ are given at discrete grid points. The conservative, or primary, variable $U(t,x)$ is replaced by its average $U_i^n$ over the cell $i$ at coordinate point $x_i$, and at the discrete time step $t^n$. The algorithms used in this work belong to the class of finite-volume methods where fluxes of the conserved quantity through the cell boundaries are calculated or approximated. This explicitly guarantees the conservation of the primary variable. The velocity and source terms are defined as a function of primary variables. Whenever source terms contain spatial derivatives, they are calculated by using second-order central differences, e.g. $\partial_x U_i^n = (U_{i+1}^n - U_{i-1}^n)/(2\Delta x)$. Time derivatives in source terms are calculated using first-order backward differences, e.g. $\partial_t U_i^n = (U_i^{n-1} - U_i^n)/\Delta t$.

Here we will give a brief presentation of our numerical algorithm. Due to its simplicity, accuracy, and easy implementation for this study we choose the SHASTA [33] which was one of the first versions of Flux Corrected Transport (FCT) algorithms in the 1970s. Ever since, the FCT method has been extensively tested and refined for various studies, for example, the ETBFCT version by Boris [34], which also forms the basis for the LCPFCT algorithm [35], and the YD-FCT algorithm by Tóth and Odstrcil [36].

These explicit higher-order monotonic numerical methods have been especially designed to work in the presence of strong gradients such as shocks. Typically low-order numerical schemes result in strong numerical diffusion due to the large truncation error, which tends to smooth out all the structures in the solution. Thus, low-order schemes are practically unusable unless unrealistically small grid sizes are used. Second-order schemes do not suffer from large numerical diffusion, but instead from a strong numerical dispersion, i.e., different Fourier modes propagate at different speeds. Especially in the presence of strong gradients like shock waves, numerical dispersion causes unphysical ripples in the solution, which eventually invalidates the whole calculation.

In the SHASTA this problem is solved by first calculating a low-order solution which has a large numerical diffusion component. In the second step, as much diffusion as possible is removed from the low-order solution in such a way that no new maxima or minima are created, i.e., the monotonicity of the solution will be preserved. The remaining, or residual, diffusion of numerical origin is called numerical viscosity. In the FCT algorithms the numerical viscosity has both linear and non-linear contributions and therefore must be assessed separately for the problems at hand. This implicit numerical viscosity is, of course, different from the well-known explicit artificial viscosity of von Neumann, or Lax and Wendroff [37].

The low-order, or transported and diffused, solution in the explicit SHASTA method [33] is given by

$$\tilde{U}_i = \frac{1}{2}\big(Q_+^2 \Delta_i - Q_-^2 \Delta_{i-1}\big) + (Q_+ - Q_-) U_i^n + \Delta t S_i. \tag{145}$$

Here, we defined

$$\Delta_i = U_{i+1} - U_i, \tag{146}$$

$$Q_\pm = \frac{1/(2\lambda) \mp v_i^n}{1/\lambda \pm (v_{i\pm1}^n - v_i^n)}, \tag{147}$$

where $\lambda \equiv \Delta t/\Delta x$ is the Courant number which in the SHASTA is restricted to values $\lambda \le 1/2$. The final time-advanced quantities are calculated by subtracting the so-called antidiffusion fluxes, $\tilde{A}$, from the transported and diffused solution such that

$$U_i^{n+1} = \tilde{U}_i - \tilde{A}_i + \tilde{A}_{i-1}, \tag{148}$$

where the flux-corrected antidiffusion flux is

$$\tilde{A}_i = \sigma_i \max\big[0, \min\big(\sigma_i \tilde{\Delta}_{i+1}, |A_i|, \sigma_i \tilde{\Delta}_{i-1}\big)\big]. \tag{149}$$

Here, similarly as in (146) the difference of primary variables in adjacent cells is denoted by $\tilde{\Delta}_i = \tilde{U}_{i+1} - \tilde{U}_i$, while the explicit antidiffusion flux is

$$A_i = A_{\mathrm{ad}} \tilde{\Delta}_i / 8, \tag{150}$$

$$\sigma_i = \mathrm{sgn}(A_i). \tag{151}$$

In the SHASTA, $A_{\mathrm{ad}} = 1$ is the default value of the so-called mask coefficient [38]. This is a multiplicative constant which can be set to lower values to reduce the amount of antidiffusion.

Second-order accuracy in time is obtained by applying the SHASTA twice. First we calculate the velocity and source terms at time step $n + 1/2$. In the second step, these half-step velocity and source terms are used to calculate the final time-advanced quantity $U_i^{n+1}$. In a given cell, this can be summarized in formulas as

$$U^{n+1/2} = U^n\big(U^n, v^n, S^n, \Delta t/2, \Delta x\big), \tag{152}$$

$$U^{n+1} = U^n\big(U^n, v^{n+1/2}, S^{n+1/2}, \Delta t, \Delta x\big). \tag{153}$$

The relaxation equations are solved in a similar manner, however in this case the source terms actually depend on the primary variables, velocity field, and LRF quantities, therefore their values must be saved for full and half time steps. This requires much more memory compared to codes which solve ideal relativistic fluid dynamics.

### 4.2 Multidimensional implementation

The $(2+1)$-dimensional conservation equations are commonly written as

$$\partial_t U + \partial_x(v_x U) + \partial_y(v_y U) = S(t,x,y). \tag{154}$$

The cell-averaged conserved variable $U(t,x,y)$ is denoted by $U^n_{i,j}$. A standard approach to solve such equations is to apply the dimensional or operator splitting method, which splits the original multidimensional equation into a sequence of $(1+1)$-dimensional problems [39].

A slightly different but more efficient approach is used in this work. We calculate the low-order transport solution separately in the $x$ and $y$ directions by using the $(1+1)$-dimensional SHASTA (145) without the source term. Thus, the $x$-transported quantity $\tilde{U}^x_{i,j}$ is given as

$$\tilde{U}^x_{i,j} = \frac{1}{2}\big[\big(Q^x_+\big)^2\Delta^x_{i,j} - \big(Q^x_-\big)^2\Delta^x_{i-1,j}\big] + \big(Q^x_+ - Q^x_-\big)U^n_{i,j}, \tag{155}$$

$$Q^x_\pm = \frac{1/(2\lambda^x) \mp (v_x)^n_{i,j}}{1/\lambda^x \pm [(v_x)^n_{i\pm1,j} - (v_x)^n_{i,j}]}, \tag{156}$$

where $\Delta^x_{i,j} = U^n_{i+1,j} - U^n_{i,j}$ and $\lambda^x = \Delta x/\Delta t \le 0.5$ is the Courant number in the $x$ direction. A similar formula, with $v_x$ replaced by $v_y$ and all cell differences taken in $y$ direction, holds for the $y$-transported quantity $\tilde{U}^y_{i,j}$. The transported and diffused solution is then

$$\tilde{U}_{i,j} = \tilde{U}^x_{i,j} + \tilde{U}^y_{i,j} - U^n_{i,j} + \Delta t\, S_{i,j}. \tag{157}$$

The advantage of this method is that it keeps the $x-y$ symmetry of the system without the need to permute the directions in which the grid is updated. In this case it is also possible to implement a multidimensional flux correction in the FCT algorithm which avoids some numerical problems and leads to slightly smoother results compared to the dimensional splitting method for the same mask coefficient. To obtain second-order accuracy, we use the method by DeVore [40], which is an improved version of Zalesak's method [41]. The full solution is given by

$$U^{n+1}_{i,j} = \tilde{U}_{i,j} - \hat{A}^x_{i,j} - \hat{A}^y_{i,j} + \hat{A}^x_{i-1,j} + \hat{A}^y_{i,j-1}, \tag{158}$$

where the $\hat{A}$'s are the limited antidiffusion fluxes given in (171) and (172) below.

As in the $(1+1)$-dimensional case the antidiffusion fluxes in $x$ and $y$ directions are given by

$$A^x_{i,j} = A^x_{\mathrm{ad}}\,\tilde{\Delta}^x_{i,j}/8, \tag{159}$$

$$A^y_{i,j} = A^y_{\mathrm{ad}}\,\tilde{\Delta}^y_{i,j}/8, \tag{160}$$

where $A^x_{\mathrm{ad}}$, $A^y_{\mathrm{ad}}$ are the antidiffusive mask coefficients, similarly to the $(1+1)$-dimensional case. Furthermore,

$$\tilde{\Delta}^x_{i,j} = \tilde{U}_{i+1,j} - \tilde{U}_{i,j}, \tag{161}$$

$$\tilde{\Delta}^y_{i,j} = \tilde{U}_{i,j+1} - \tilde{U}_{i,j}. \tag{162}$$

In the DeVore scheme, the antidiffusion fluxes in $x$ and $y$ directions are first limited as in the $(1+1)$-dimensional case,

$$\tilde{A}^x_{i,j} = \sigma^x_{i,j}\max\big[0, \min\big(\sigma^x_{i,j}\tilde{\Delta}^x_{i+1,j}, |A^x_{i,j}|, \sigma^x_{i,j}\tilde{\Delta}^x_{i-1,j}\big)\big], \tag{163}$$

$$\tilde{A}^y_{i,j} = \sigma^y_{i,j}\max\big[0, \min\big(\sigma^y_{i,j}\tilde{\Delta}^y_{i,j+1}, |A^y_{i,j}|, \sigma^y_{i,j}\tilde{\Delta}^y_{i,j-1}\big)\big], \tag{164}$$

where $\sigma^x_{i,j} = \mathrm{sgn}(A^x_{i,j})$ and $\sigma^y_{i,j} = \mathrm{sgn}(A^y_{i,j})$. Note that this additional step was introduced by DeVore into the multidimensional flux limiting algorithm by Zalesak.

The allowed values for $U^{n+1}_{i,j}$ after the antidiffusion stage are between

$$\tilde{U}^{\min}_{i,j} = \min\big(\tilde{U}_{i,j-1}, \tilde{U}_{i-1,j}, \tilde{U}_{i,j}, \tilde{U}_{i+1,j}, \tilde{U}_{i,j+1}\big), \tag{165}$$

$$\tilde{U}^{\max}_{i,j} = \max\big(\tilde{U}_{i,j-1}, \tilde{U}_{i-1,j}, \tilde{U}_{i,j}, \tilde{U}_{i+1,j}, \tilde{U}_{i,j+1}\big). \tag{166}$$

The total incoming and outgoing antidiffusive fluxes in cell $(i,j)$ are calculated as

$$A^{\mathrm{in}}_{i,j} = \max\big(0, \tilde{A}^x_{i-1,j}\big) - \min\big(0, \tilde{A}^x_{i,j}\big) + \max\big(0, \tilde{A}^y_{i,j-1}\big) - \min\big(0, \tilde{A}^y_{i,j}\big), \tag{167}$$

$$A^{\mathrm{out}}_{i,j} = \max\big(0, \tilde{A}^x_{i,j}\big) - \min\big(0, \tilde{A}^x_{i-1,j}\big) + \max\big(0, \tilde{A}^y_{i,j}\big) - \min\big(0, \tilde{A}^y_{i,j-1}\big). \tag{168}$$

This information is then used to determine the fractions of the incoming and outgoing fluxes,

$$F^{\mathrm{in}}_{i,j} = \big(\tilde{U}^{\max}_{i,j} - \tilde{U}_{i,j}\big)/A^{\mathrm{in}}_{i,j}, \tag{169}$$

$$F^{\mathrm{out}}_{i,j} = \big(\tilde{U}_{i,j} - \tilde{U}^{\min}_{i,j}\big)/A^{\mathrm{out}}_{i,j}, \tag{170}$$

which is subsequently limited so that it creates no undershoot or overshoot in the cell it is leaving or entering. Thus, the new antidiffusive fluxes are given as

$$\hat{A}^x_{i,j} = \tilde{A}^x_{i,j} \times \begin{cases} \min(1, F^{\mathrm{in}}_{i+1,j}, F^{\mathrm{out}}_{i,j}), & \text{if } \tilde{A}^x_{i,j} \ge 0, \\ \min(1, F^{\mathrm{in}}_{i,j}, F^{\mathrm{out}}_{i+1,j}), & \text{if } \tilde{A}^x_{i,j} < 0, \end{cases} \tag{171}$$

and

$$\hat{A}^{y}_{i,j} = \tilde{A}^{y}_{i,j} \times \begin{cases} \min(1, F^{\text{in}}_{i,j+1}, F^{\text{out}}_{i,j}), & \text{if } \tilde{A}^{y}_{i,j} \geq 0, \\ \min(1, F^{\text{in}}_{i,j}, F^{\text{out}}_{i,j+1}), & \text{if } \tilde{A}^{y}_{i,j} < 0. \end{cases} \quad (172)$$

This $(2+1)$-dimensional numerical scheme can be generalized to $(3+1)$ dimensions by extending the method to another spatial direction and repeating the above steps.

### 4.3 Other numerical schemes

Computational fluid dynamics (CDF) is a constantly growing field of research. There is a vast amount of methods which have been designed to solve the special relativistic fluid-dynamical equations in the perfect-fluid limit, see Refs. [42, 43] and references therein.

In applications to relativistic heavy-ion collision the FCT-SHASTA and RHLLE methods have been systematically explored for various test problems and shown to give excellent agreement [44–46]. This is one of the reasons why we have chosen the SHASTA for our study. There are other well-known methods widely used in astrophysics and heavy-ion physics, such as Smoothed-Particle Hydrodynamics (SPH) [47, 48] which has been recently extended to dissipative fluids [49–52], or the Particle-In-Cell (PIC) method [53, 54], but since they are completely different from finite-volume schemes we will not go into details.

Other methods of interest such as High-Resolution Shock-Capturing (HRSC) methods based on the exact or approximate Riemann solution proved to be superior to SHASTA [42–44, 55]. However, in case of dissipative fluids such methods become difficult to apply due to the fact that there are no known analytic or approximate solutions for the Riemann problem. Recently, new methods have been developed to solve the hyperbolic equations of conservation or relaxation type which sidestep the need of Riemann solvers but have an accuracy comparable to HRSC schemes. These are new High-Resolution Central Schemes (HRCS) improving on the Lax–Friedrichs central scheme [56]. The most important of these are the Nessayu–Tadmor (NT) [57] and the Kurganov–Tadmor (KT) [58] schemes, see Ref. [59] for a collection of references.

The KT scheme improves upon the NT scheme using information about the local propagation of speeds, which becomes problematic to evaluate for the IS equations. However, it gives excellent results for perfect fluids [60]. An important extension of the NT scheme was made by Pareschi [61] to describe both the stiff and unstiff regions of hyperbolic relaxation equations such as the IS equations or equations of Öttinger–Grmela type [62]. In the latter case, this method has been shown to provide robust results and excellent agreement between the $(1+1)$- and $(2+1)$-dimensional cases [63]. Following this work we also made use of both the NT and KT schemes and compared them with SHASTA for the $(1+1)$-dimensional evolution of a perfect fluid. The results are very robust and agree very well. Therefore, without much more efficient methods at hand we simply choose to solve the IS equations with the SHASTA.

### 4.4 Remarks on numerical resolution

Fluid dynamics is a theory which is valid on time and length scales which are larger than the underlying microscopic time and length scales. In solving the equations of fluid dynamics numerically, we should be able to resolve all relevant time and length scales in the problem. In practice this means that the grid spacing $\Delta x$ and time step $\Delta t$ should be smaller than any of these scales. In perfect-fluid dynamics, or in the Navier–Stokes theory, all scales are macroscopic, i.e., they are inversely proportional to the gradients of the fluid-dynamical variables like flow field and densities. Thus it is sufficient to have a numerical resolution that correctly resolves the macroscopic structures.

In the IS theory we also need to solve the relaxation equations for the dissipative currents. In this case the relevant time scale to be resolved is the relaxation time $\tau_R$, which is of the order of the mean time between the collision of particles. Thus, the time step should be chosen such that $\Delta t \ll \tau_R$. If $\tau_R$ is much smaller than the macroscopic scales, this might require very high resolution and therefore lead to very demanding calculations. However, in modeling heavy-ion collisions, an application which we mainly have in mind, scale separation by several orders of magnitude is not expected throughout the whole fluid-dynamical evolution.

There exist specialized methods [61] to solve the equations in stiff regions. However, we do not consider these methods here, but simply choose sufficiently high resolution to resolve both the macroscopic and relaxation time scales. Therefore, we solve simultaneously both the conservation and the relaxation equations with the same numerical resolution and scheme.

### 4.5 Remarks on dissipative fluxes

In relativistic dissipative fluid dynamics, the components of $T^{\mu\nu}$ and $\pi^{\mu\nu}$ cannot take arbitrary values. Obvious physical constraints are that the LRF energy density must be positive semi-definite and the velocity must be bounded from above by the speed of light, i.e., $e \geq 0$ and $v \leq 1$. Another constraint follows from the equation for energy conservation,

$$\partial_\mu T^{0\mu} = \partial_t T^{00} + \nabla \cdot \left(\tilde{\mathbf{v}} T^{00}\right) = 0, \quad (173)$$

where $\tilde{v}^i \equiv T^{0i}/T^{00}$. In order to have causal propagation of energy, we have to require that $|\tilde{\mathbf{v}}| \leq 1$, i.e.,

$$\sqrt{-T^{0i}T_{0i}} \leq T^{00}. \quad (174)$$

For perfect fluids, because of (49), this condition guarantees both $e \geq 0$ and $v \leq 1$, provided that the pressure is positive. However, in dissipative fluid dynamics this is not necessarily true, since the condition (174) is sufficient only if the effective pressure is positive. For example, neglecting the shear pressure this leads to the condition $\Pi > -p$ for the bulk viscous pressure.

The IS theory does not itself restrict the values of the dissipative quantities. In principle any value of shear and bulk pressure can be used, e.g. as an initial condition. However, the applicability of the theory requires that the dissipative currents give sufficiently small corrections to the equilibrium quantities. For the shear and bulk pressure this requirement can be stated as

$$|\Pi| < Cp, \tag{175}$$

$$\left|\pi^{\mu\nu}\right| < C\left|T^{\mu\nu}_{\mathrm{eq}}\right|, \tag{176}$$

where $C$ is a constant of order, but smaller than, one. If these conditions are not satisfied, fluid dynamics is not expected to give a reasonable description of the space-time evolution of the system and the numerical calculation can become unstable [32]. To protect the code from these numerical instabilities the conditions (175) and (176) are always enforced. This means that after each time step the above conditions are checked and $\pi^{\mu\nu}$ and $\Pi$ are adjusted accordingly. We note that the above conditions may be enforced before the velocity root search, in which case we have to compare to the values of $T^{\mu\nu}_{\mathrm{eq}}$ and $p$ from the previous time step. Alternatively, one can apply these limiters inside the root search algorithm. In this case the limiters are applied simultaneously with solving for the LRF densities and the velocity. In every iteration of the velocity root search the shear and bulk viscous pressure are compared to the values of $T^{\mu\nu}_{\mathrm{eq}}$ and $p$ at the current time level. This guarantees that the conditions are always fulfilled, but the drawback is that this is computationally more expensive. In situations where we expect fluid dynamics to give a reasonable description these conditions need not be enforced. However, if they are violated only in small regions of space-time, i.e., few cells or few time steps, enforcing the inequalities can prevent these regions to invalidate the whole calculation. Naturally, if the inequalities are violated in large regions of space-time, it signals that fluid dynamics is no longer a valid theory for such situations.

## 5 Results of comparisons

In this section we apply the different numerical schemes described above to the relativistic Riemann problem in $(1+1)$ and $(2+1)$ dimensions. In $(1+1)$ dimensions the Riemann problem is analytically solvable for perfect fluids. Thus, it provides an important test case to compare the performance and accuracy of different numerical algorithms.

Unfortunately, analytic solutions for the one-dimensional viscous Riemann problem are, to the best of our knowledge, not known. However, this type of one-dimensional test was performed previously: our fluid-dynamical calculations with non-zero viscosity were shown to give good agreement with kinetic-theory simulations using the Boltzmann Approach to MultiParton Scatterings (BAMPS) [64] parton cascade code [65, 66]. The purpose of our tests here are to show that a more complex $(2+1)$-dimensional code can, with similar initial conditions, remarkably well reproduce our earlier results for $(1+1)$ dimensions. This confirms that the numerical method produces correct answers in these test scenarios, and gives us confidence that it can be successfully used to study phenomena where dissipation plays an important role.

We shall proceed as follows: First, the Riemann problem is briefly introduced and its analytic solution in $(1+1)$ dimensions is compared with numerical solutions in the perfect-fluid limit. Here we compare the SHASTA, the NT, and the KT numerical schemes. They all give comparable results and can reproduce the analytic results with sufficiently good numerical resolution. This gives confidence that any of the schemes forms a good basis to extend the calculation to multidimensional problems as well as to non-zero viscosity. In this work these extensions are made by using the SHASTA.

Second, the numerical solutions for the $(1+1)$-dimensional Riemann problem with non-zero shear viscosity are shown. We compare results from the $(2+1)$-dimensional code to the results from the $(1+1)$-dimensional code and show that both codes yield, to good accuracy, the same results.

Finally, the numerical solutions of the $(2+1)$-dimensional, azimuthally symmetric Riemann problem with non-zero shear viscosity are studied. We compare the results from the $(1+1)$-dimensional azimuthally symmetric code to the results from the $(2+1)$-dimensional code. Again, these calculations are in excellent agreement with each other.

### 5.1 The Riemann problem

The initial setup for the $(1+1)$-dimensional Riemann problem consists of two states with constant pressure, $p_0$ and $p_4$, separated by a membrane at $z = 0$. The matter is initially at rest on both sides and homogeneous in the transverse directions. After the membrane is removed, in thermodynamically normal matter [45] there is a shock wave traveling into the region with lower pressure, and a rarefaction fan into the region with larger pressure. The interface between the two regions moves at a constant velocity and is called the shock plateau. In dissipative fluids due to non-zero viscosity the initial sharp discontinuity will be smeared out and the quantities will change smoothly rather than discontinuously.

In numerical calculations, unless stated otherwise, we have fixed the parameters as follows: The local Courant

number is $\lambda^x = \lambda^y = 0.4$, and the comparison is made at $t = 4$ fm. The cell sizes $\Delta x$, $\Delta y$, and the antidiffusion coefficients, $A^x_{\rm ad}$, $A^y_{\rm ad}$ are specified separately in all cases.

The energy density in local equilibrium is given by $e = \frac{3g}{\pi^2}T^4$ where $g = 16$ is the number of degrees of freedom. Therefore, on the left- and right-hand side of the initial discontinuity the energy densities correspond to the following temperatures: on the left $T_0 = 0.4$ GeV and on the right $T_4 = 0.2$ GeV. The bulk viscosity to entropy density ratio $\zeta/s$ and the shear viscosity to entropy density ratio $\eta/s$ are taken as a constant, where the entropy density $s = s_{\rm eq}$ is fixed to its equilibrium value, $s_{\rm eq} = \frac{4g}{\pi^2}T^3$. In all test cases we start from local thermal equilibrium, i.e., initially $\pi^{\mu\nu} = 0$. We show only results with shear viscosity, but we have tested that we get similar results with non-zero bulk viscous pressure.

### 5.2 Comparing different methods in perfect-fluid dynamics

The first test compares how well the different numerical methods can reproduce the analytic Riemann solution [44] in the perfect-fluid limit. The left panel of Fig. 1 shows the velocity $v$, the LRF energy density $e$, and the expansion rate $\theta$ calculated with the SHASTA, the NT, and the KT schemes compared with the analytic solution. The numerical calculations in the figure are made with cell size $\Delta x = 0.1$ fm and $\Delta t = 0.04$ fm/c. We used the non-staggered version of the HRCS schemes with a minmod limiter ($\theta = 2$) which ensures that no local extrema are introduced, see (4.9) in Ref. [58].

All algorithms reproduce the analytic solution with nearly the same accuracy and numerical artefacts. In particular, all methods show long-wavelength oscillations which are best visible in the expansion rate, in the region between the rarefaction tail and the shock wave. The HRCS calculations show a somewhat larger overshoot for the velocity at the contact discontinuity as well as a more diffused shock front compared to SHASTA with $A_{\rm ad} = 1.0$.

We also compared the above SHASTA result with a calculation with a reduced mask coefficient $A_{\rm ad} = 0.8$, shown in the right panel of Fig. 1. This reduction strongly suppressed the unphysical oscillations in the numerical solution, but leads also to more diffusive profiles. Furthermore, with the standard mask coefficient we have used the viscous

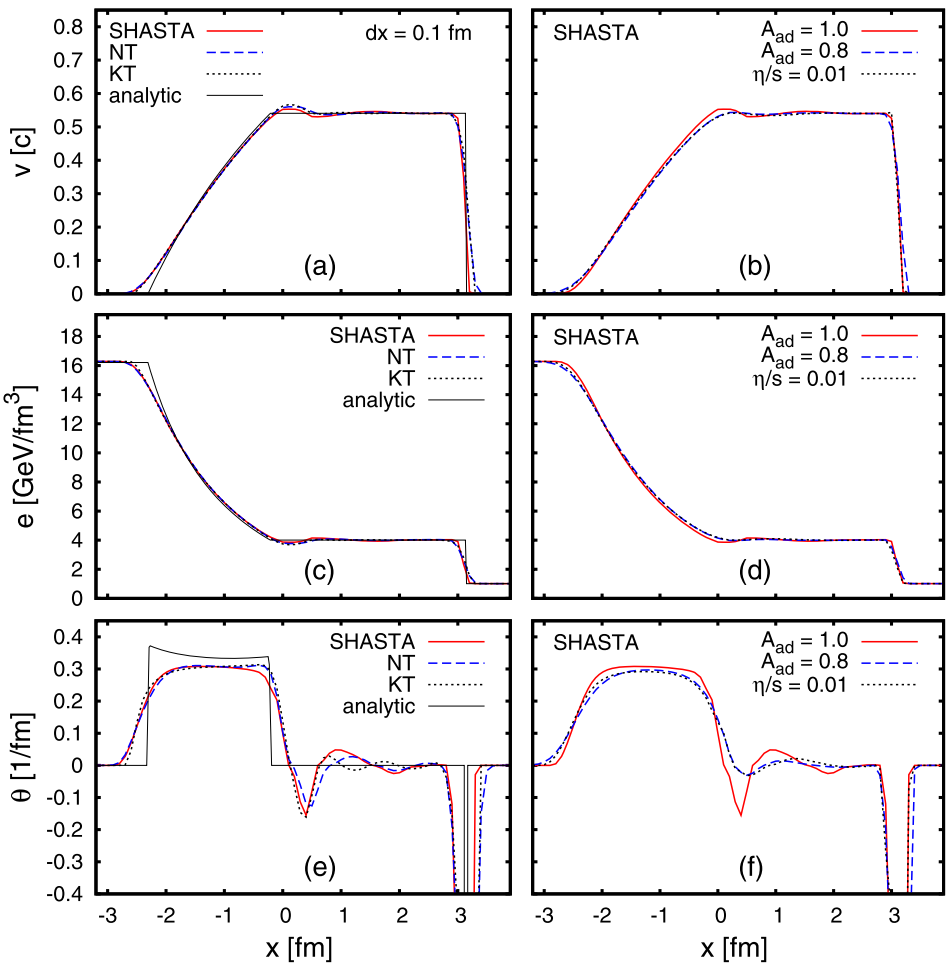


**Fig. 1** (Color online) The analytic (*thin line*) and numerical solutions of the relativistic Riemann problem on a grid with $N_x = 100$ cells with $\Delta x = 0.1$ fm, after $N_t = 100$ time steps at $t = 4$ fm/c. **a** the collective flow velocity of matter, $v$, calculated with the SHASTA (*continuous line*), and the NT (*dashed line*) and KT (*dotted line*) algorithms. **b** The velocity, $v$, calculated with SHASTA using a mask coefficient $A_{\rm ad} = 1.0$ (*continuous line*), $A_{\rm ad} = 0.8$ (*dashed line*), and vSHASTA with $A_{\rm ad} = 1.0$ and $\eta/s = 0.01$ (*dotted line*). Similarly, the LRF energy density, $e$, and the invariant expansion rate, $\theta$, are shown in the panels **c**, **d**, and **e**, **f**, respectively

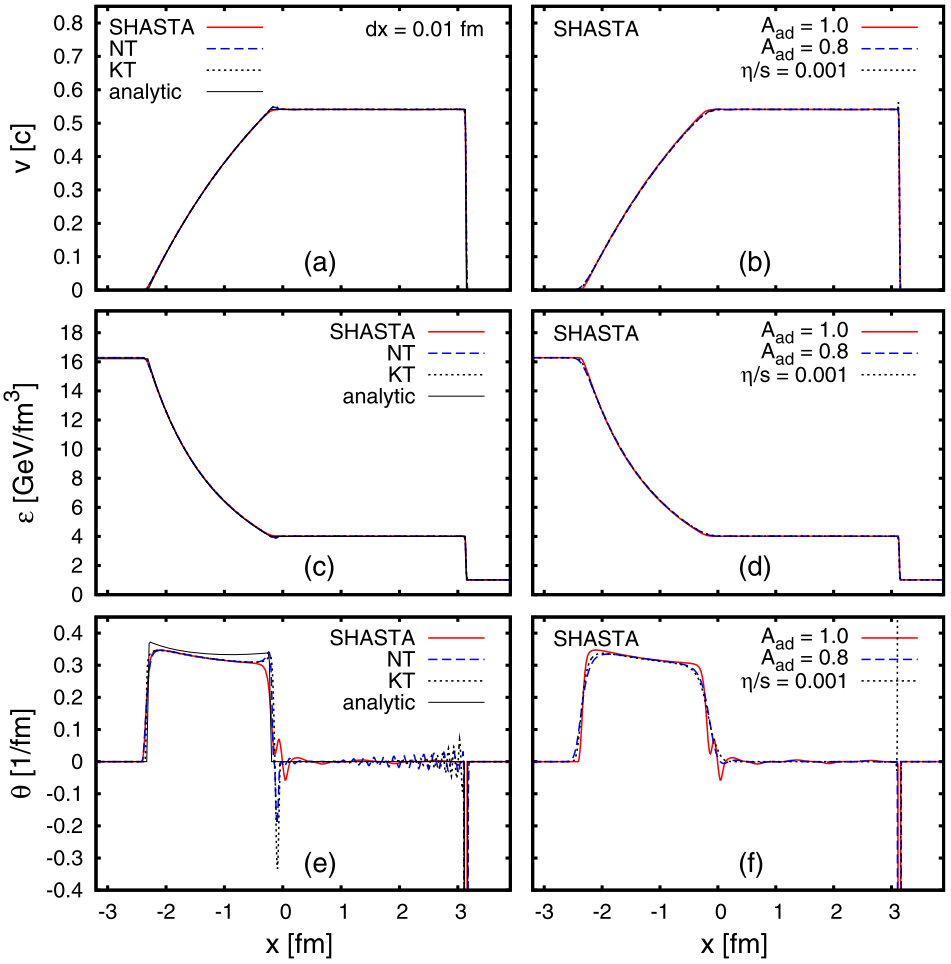


**Fig. 2** (Color online) As in Fig. 1, except for $N_x = 1000$ cells with $\Delta x = 0.01$ fm, after $N_t = 1000$ time steps at $t = 4$ fm/c. Analogously, the shear viscosity to entropy density ratio in the vSHASTA calculations shown in panels **b**, **d**, **f** is $\eta/s = 0.001$

SHASTA (vSHASTA)[2] solver with a small physical viscosity $\eta/s = 0.01$ and $A_{\mathrm{ad}} = 1.0$. This very closely reproduces the $A_{\mathrm{ad}} = 0.8$ results with $\eta/s = 0$, especially at the smooth parts of the solution. Therefore, albeit small discrepancies exist at the shock font, we can conclude that our numerical solutions with the reduced antidiffusion mask coefficient have an additional numerical viscosity corresponding to $\eta/s \approx 0.01$ compared to the $A_{\mathrm{ad}} = 1.0$ case.

Since all numerical calculations only approximate the exact solution, there is always some residual numerical viscosity in the solution. In fact, some amount of numerical viscosity is required to stabilize the solution. However, this residual numerical viscosity can be made arbitrary small by increasing the resolution. This is demonstrated in Figs. 2a, c, e, where all numerical algorithms considered reproduce the analytic solution almost perfectly with a cell size of $\Delta x = 0.01$ fm and $\Delta t = 0.004$ fm/c. Also, the additional numerical viscosity resulting from the reduction of the mask coefficient $A_{\mathrm{ad}}$ scales approximately with the cell size for a constant Courant number. This is demonstrated in the right panel of Fig. 2, where we found that the additional numerical viscosity corresponds to $\eta/s \approx 0.001$. We have checked that we get similar results also with other initial temperature ratios.

### 5.3 Comparison between the one- and two-dimensional solutions

The next numerical tests consist of comparing the $(1+1)$-dimensional solution to the $(2+1)$-dimensional solution of the one-dimensional Riemann problem in Cartesian coordinates. The one-dimensional Riemann problem can be initialized on a two-dimensional grid in several different ways. We study here two different initializations. In the first case, the initial discontinuity is along the $y$ axis, i.e., on the $x = 0$ plane. In the second case we place the discontinuity on the $y = -x$ plane. These two cases are compared to the $(1+1)$-dimensional calculation. Here both one- and two-dimensional calculations are done using the vSHASTA algorithm, with $A_{\mathrm{ad}} = 0.8$, grid size $\Delta x = 0.2$ fm and non-zero shear viscosity $\eta/s = 0.1$ in all cases.

[2] Our abbreviation only specifies that next to the conservation equations we also solve the relaxation equations of the physical viscosity using SHASTA.

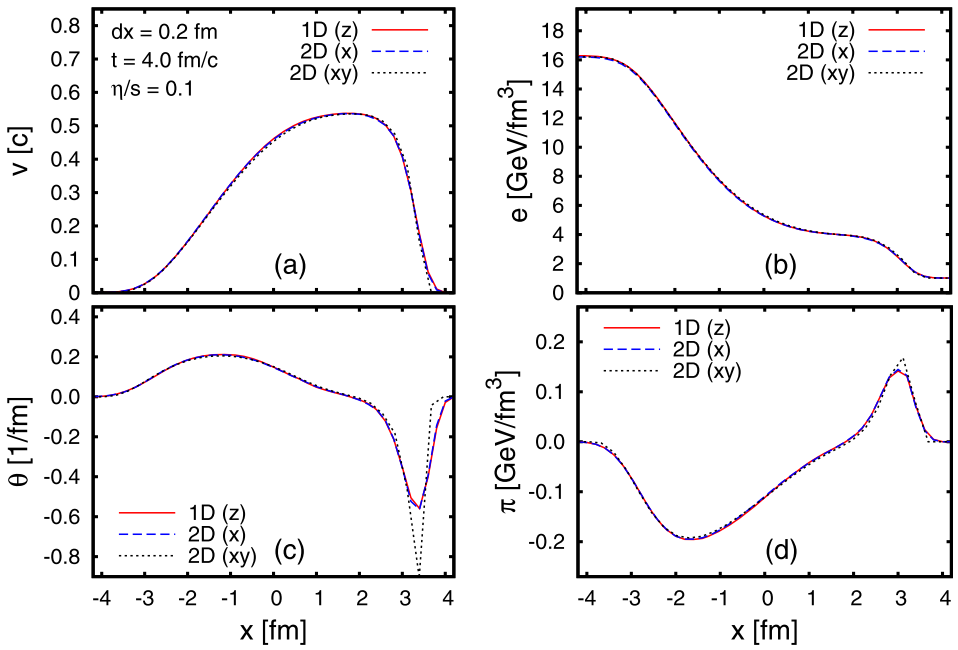


**Fig. 3** (Color online) The numerical solution of the relativistic Riemann problem with $\eta/s = 0.1$ on a symmetric grid with $N_x = N_y = 200$ cells with $\Delta x = 0.2$ fm, after $N_t = 50$ time steps at $t = 4$ fm/c. In all figures, the *full line* shows the one-dimensional evolution of matter. The *dashed line* shows the two-dimensional solution in $x$ direction, while the *dotted line* shows the solution in the diagonal $x = y$ direction. **a** The collective flow velocity of matter, $v$, **b** the LRF energy density, $e$, **c** the invariant expansion rate $\theta$, and **d** the shear viscous pressure, $\pi$

In the simple one-dimensional formulation, there are only two dissipative quantities to propagate, $\Pi_1$ and $\pi_1$, while the other shear stress tensor components are straightforward to calculate. In the two-dimensional setup we always propagate all non-vanishing dissipative tensor components, $\Pi_2, \pi_2^{00}, \pi_2^{0x}, \pi_2^{0y}, \pi_2^{xx}, \pi_2^{yy}, \pi_2^{xy}, \pi_2^{zz}$. Because there is only one independent shear stress component $\pi$ in the one-dimensional Riemann problem, any of the non-vanishing shear stress components in the two-dimensional calculations can be used to extract $\pi$. The simplest possibility is to use $\pi = -2\pi^{zz}$, because $\pi^{zz}$ is independent of the orientation of the initial state in the $(x, y)$-plane.

The result of the comparison between the one- and the two-dimensional calculations is shown in Fig. 3, where we compare the velocity $v$, the LRF energy density $e$, the expansion rate $\theta$, and the shear pressure $\pi$. The velocity $v = v_z$ in the one-dimensional calculation, while $v = v_x$ or $v = \sqrt{v_x^2 + v_y^2}$ in the two-dimensional cases. In the two-dimensional calculations the quantities are plotted along the $x$ axis when the initial discontinuity is at $x = 0$, or along the $y = x$ line when the discontinuity is in the $y = -x$ plane.

When the initial discontinuity is in the $x = 0$ plane the two-dimensional SHASTA reduces essentially to the one-dimensional one. This is because there are no gradients in the $y$ direction and $v_y = 0$. Therefore, in this case we expect very good agreement between the one- and two-dimensional calculations. This is confirmed in Fig. 3, where the two-dimensional calculation (dashed line) is basically on top of the one-dimensional calculation (solid line).

When the initial discontinuity is along the $y = -x$ plane, there are gradients in both $x$ and $y$ directions and both velocity components $v_x$ and $v_y$ are non-zero. This calculation is shown as dotted line in Fig. 3. The agreement with the $(1 + 1)$-dimensional results is still very good, although the two-dimensional algorithm gives somewhat sharper profiles in the shock region.

The next test compares the $(1 + 1)$-dimensional solution in cylindrically symmetric coordinates from Sect. 3.2 against the two-dimensional solution in Cartesian coordinates with cylindrically symmetric initial conditions. This tests how well the two-dimensional system keeps its symmetry in time and performs compared to the one-dimensional counterpart.

The initial discontinuity lies on a circle with radius $r_0 = 5$ fm, with a cell size of $\Delta r = 0.2$ fm in both cases. The velocity and position in the one-dimensional case is $v = v_r$ and $x = r$, while in the two-dimensional case $v = \sqrt{v_x^2 + v_y^2}$ and $r = \sqrt{x^2 + y^2}$. The first two-dimensional result compares the evolution of the system along the $x$ axis, i.e., $y = 0$, while the second one does this along the diagonal, $x = y$. These are plotted with dashed and dotted lines, respectively, against the one-dimensional solution (solid line) in Fig. 4. The other plots show the expansion rate, and the shear stress tensor components, $\pi^{zz}$, $r^2\pi^{\phi\phi}$, and $\pi^{0r}$ as calculated from the different equations in Sects. 3.2 and 3.3.

Similarly as before, the results are nearly the same, however, differences in the diagonal direction are visible and more pronounced than along the coordinate axis, due to the finite resolution. The agreement will obviously get better by decreasing the cell size and time step.

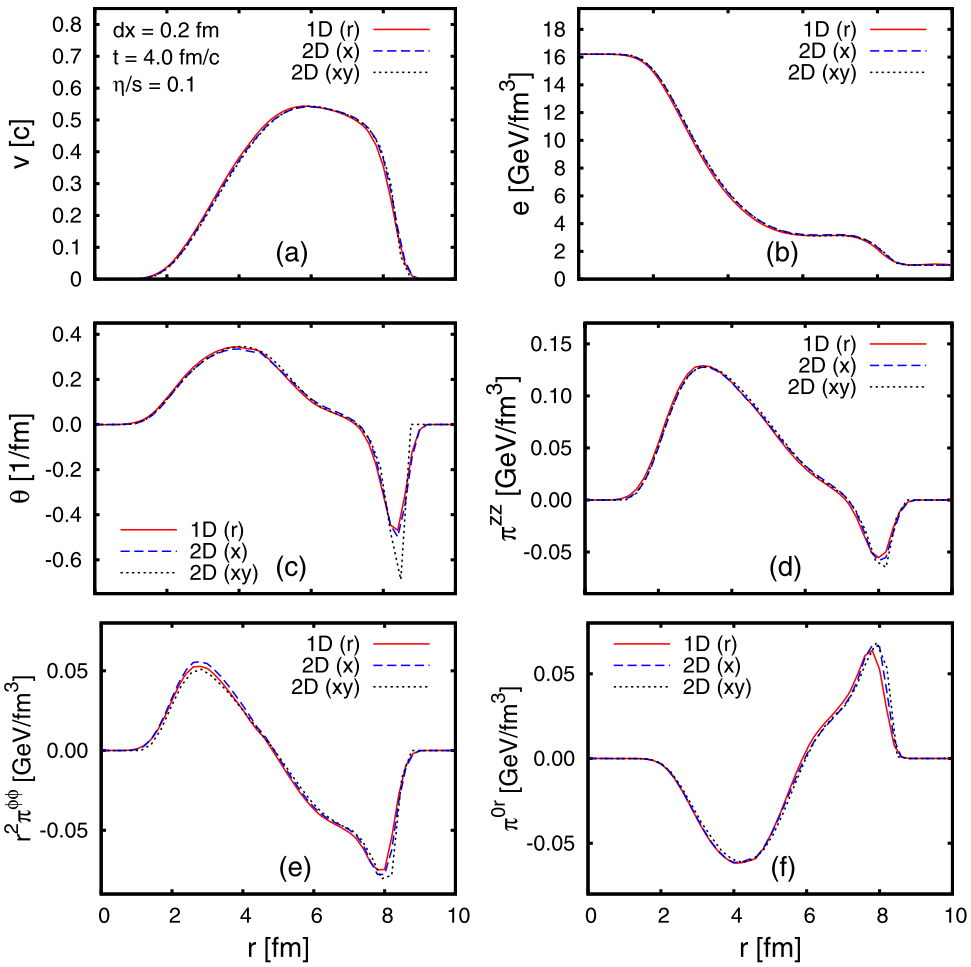


**Fig. 4** (Color online) The numerical solution of the relativistic Riemann problem in cylindrical geometry, with $\eta/s = 0.1$ on a symmetric grid with $N_x = N_y = 200$ cells with $\Delta x = 0.2$ fm, after $N_t = 50$ time steps at $t = 4$ fm/c. In all figures, the *full line* shows the one-dimensional evolution of matter. The *dashed line* shows the two-dimensional solution in the $x$ direction, while the *dotted line* shows the solution in the diagonal $x = y$ direction. **a** The collective flow velocity of matter, $v$, **b** the LRF energy density, $e$, and **c** the invariant expansion rate, $\theta$. The shear stress components $\pi^{zz}$, $r^2\pi^{\phi\phi}$, and $\pi^{0r}$ are shown in panels **d**, **e**, and **f**, respectively

## 6 Conclusions

In this paper, we have studied numerical algorithms to solve the IS theory for relativistic dissipative fluid dynamics. First, we briefly reviewed the IS theory and wrote the IS equations for $(1+1)$- and $(2+1)$-dimensional systems in Cartesian coordinates, and for $(1+1)$-dimensional azimuthally symmetric systems in cylindrical coordinates. For the sake of completeness we present the $(3+1)$-dimensional equations in Cartesian coordinates and the $(2+1)$-dimensional boost-invariant and $(3+1)$-dimensional equations in $(\tau, x, y, \eta)$ coordinates in the Appendices. We also gave a detailed introduction to the FCT-SHASTA method for one and multidimensional applications, together with a brief discussion on the HRCS methods NT and KT. We also discussed relationship between microscopic and macroscopic scales, as well as physical limitations for the components of the energy–momentum tensor.

In our first numerical comparison we solved the $(1+1)$-dimensional Riemann problem in the perfect-fluid limit. This problem has an analytic solution which allowed us to make a definite comparison of performance and accuracy of the different numerical algorithms. For this problem all the algorithms considered here, i.e., the NT, KT, and SHASTA methods, gave very similar results. All of them could reproduce the analytic solution with a very high precision with sufficiently high numerical resolution. Moreover, with the same resolution the accuracy of the methods was found to be similar, i.e., none of them showed significantly faster convergence to the analytic solution when the grid spacing was decreased. For this reason we have chosen SHASTA for all the other geometries as well as for all calculations with non-zero viscosity.

We further studied the effect of the mask coefficient $A_{\mathrm{ad}}$ in the SHASTA. This numerical parameter controls the amount of numerical diffusion in the algorithm. It was found that a reduction of the coefficient by 20% from the default value smoothens unphysical sharp structures in the solution, especially in the expansion rate, and at the same time only increases the numerical viscosity by a small amount.

In the case of non-zero viscosity, the analytic solution to the Riemann problem is not known. However, we have demonstrated earlier that our $(1+1)$-dimensional code is in good agreement with kinetic-theory calculations [65, 66]. In

this work we have first applied both $(1+1)$– and $(2+1)$-dimensional Cartesian implementations of the code to the same $(1+1)$-dimensional Riemann problem. In this case we have chosen a non-zero shear viscosity, $\eta/s = 0.1$. If the discontinuity in the initial energy-density profile was chosen to be along one of the coordinate axes, perfect agreement between the one- and the two-dimensional codes was found. In the case where the initial discontinuity was chosen to be along the $y = -x$ plane, a slight difference between the two codes near the shock front was found. The results were shown for a rather large grid spacing $\Delta x = 0.2$ fm; the agreement was found to improve significantly for smaller grid spacing. A similar comparison between the $(1+1)$-dimensional solution in cylindrical coordinates versus the $(2+1)$-dimensional solution in Cartesian coordinates with cylindrically symmetric initial condition confirmed that our method works well also for problems in more than one spatial dimension.

In this work, we have demonstrated the applicability of FCT-SHASTA to solve the conservation equations of causal relativistic dissipative fluid dynamics simultaneously with relaxation transport equations. In the future, we intend to extend this method to full $(3+1)$-dimensional geometries. We plan a detailed comparison with calculations done in the framework of kinetic theory [67], as well as studies of collective flow in relativistic heavy-ion collisions.

**Acknowledgements** The authors would like to thank L.P. Csernai and A. Dumitru for useful discussions, and P. Huovinen for reading the manuscript and valuable comments.

E. Molnár gratefully acknowledges partial support by the Alexander von Humboldt foundation. H. Niemi was supported by the Extreme Matter Institute (EMMI). This work was supported by the Helmholtz International Center for FAIR within the framework of the LOEWE program launched by the State of Hesse.

## Appendix A: $(2+1)$-dimensional boost-invariant expansion

Because it is very important for modeling ultrarelativistic heavy-ion collisions, we discuss the $(2+1)$-dimensional boost-invariant equations of motion. The metric tensors are $g^{\mu\nu} = \mathrm{diag}(1,-1,-1,-1/\tau^2)$ and $g_{\mu\nu} = \mathrm{diag}(1,-1,-1,-\tau^2)$, leading to $g = \tau^2$, where $\tau = (t^2 - z^2)^{-1/2}$ is the longitudinal proper time and $\eta = 1/2\ln[(t+z)/(t-z)]$ is the space-time rapidity (which is not to be confused with the shear viscosity coefficient). The only non-vanishing Christoffel symbols are $\Gamma^{\eta}_{\eta\tau} = \Gamma^{\eta}_{\tau\eta} = \tau^{-1}$ and $\Gamma^{\tau}_{\eta\eta} = \tau$.

The equations of relativistic dissipative fluid dynamics can be easily derived from the results in Cartesian coordinates, cf. Sect. 3.3. In order to obtain the equations for the boost-invariant case, the indices for time $t$ and spatial $z$ direction have to be replaced by $\tau$ and $\eta$ in the four-vector and tensor components, $(0,x,y,z) \to (\tau,x,y,\eta)$. Therefore, we easily find that all laboratory frame quantities can be written in the same way as in (94)–(102), with the exception of the term in (103), which becomes, $T^{zz} \to T^{\eta\eta} \equiv P/\tau^2 + \pi^{\eta\eta}$. This means that $N^{\eta} = 0$, $T^{\tau\eta} = T^{x\eta} = T^{y\eta} = 0$, and $\pi^{\tau\eta} = \pi^{x\eta} = \pi^{y\eta} = 0$.

The LRF charge density, energy density, and velocity are calculated the same way as in Sect. 3.3. The charge conservation equation is

$$\partial_\tau N^\tau + \partial_x\big(v_x N^\tau\big) + \partial_y\big(v_y N^\tau\big) = -\frac{1}{\tau} N^\tau. \tag{A.1}$$

The energy conservation equation follows from $\frac{1}{\sqrt{g}}\partial_\mu(\sqrt{g}\,T^{\mu\tau}) + \Gamma^{\tau}_{\mu\beta}T^{\mu\beta} = 0$, thus

$$\begin{aligned}&\partial_\tau T^{\tau\tau} + \partial_x\big(v_x T^{\tau\tau}\big) + \partial_y\big(v_y T^{\tau\tau}\big)\\ &\quad= -\partial_x\big(v_x P - v_x\pi^{\tau\tau} + \pi^{\tau x}\big) - \partial_y\big(v_y P - v_y\pi^{\tau\tau} + \pi^{\tau y}\big)\\ &\qquad - \frac{1}{\tau}\big(T^{\tau\tau} + P + \tau^2\pi^{\eta\eta}\big).\end{aligned} \tag{A.2}$$

The momentum conservation equations follow from $\frac{1}{\sqrt{g}}\partial_\mu(\sqrt{g}\,T^{\mu i}) + \Gamma^{i}_{\mu\beta}T^{\mu\beta} = 0$:

$$\begin{aligned}&\partial_\tau T^{\tau x} + \partial_x\big(v_x T^{\tau x}\big) + \partial_y\big(v_y T^{\tau x}\big)\\ &\quad= -\frac{1}{\tau}T^{\tau x} - \partial_x\big(P - v_x\pi^{\tau x} + \pi^{xx}\big)\\ &\qquad - \partial_y\big(-v_y\pi^{\tau x} + \pi^{xy}\big),\end{aligned} \tag{A.3}$$

$$\begin{aligned}&\partial_\tau T^{\tau y} + \partial_x\big(v_x T^{\tau y}\big) + \partial_y\big(v_y T^{\tau y}\big)\\ &\quad= -\frac{1}{\tau}T^{\tau y} - \partial_x\big(-v_x\pi^{\tau y} + \pi^{xy}\big)\\ &\qquad - \partial_y\big(P - v_y\pi^{\tau y} + \pi^{yy}\big).\end{aligned} \tag{A.4}$$

The use of boost-invariant coordinates affects the expansion rate, $\theta_\perp = \gamma_\perp/\tau + \partial_\tau\gamma_\perp + \partial_x(\gamma_\perp v_x) + \partial_y(\gamma_\perp v_y)$, and the $\sigma^{zz}$ component of the shear tensor, which is replaced by $\sigma^{\eta\eta} \equiv \tau^{-2}(\theta_\perp/3 - \gamma_\perp/\tau)$. The convective time derivative $D$ from Sect. 3.3 becomes $D \equiv \gamma_\perp\partial_\tau + \gamma_\perp v_x\partial_x + \gamma_\perp v_y\partial_y$. The relaxation equations are the same as in Cartesian coordinates except for the replacement $\pi^{zz} \to \pi^{\eta\eta}$ which due to a non-vanishing Christoffel symbol includes a new term, $2\pi^{\eta\eta}\gamma_\perp/\tau$. Thus,

$$\begin{aligned}&\gamma_\perp\partial_t\pi^{\eta\eta} + \gamma_\perp v_x\partial_x\pi^{\eta\eta} + \gamma_\perp v_y\partial_y\pi^{\eta\eta}\\ &\quad= -2\pi^{\eta\eta}\frac{\gamma_\perp}{\tau} + \frac{1}{\tau_\pi}\big(\pi^{\eta\eta}_{\mathrm{NS}} - \pi^{\eta\eta}\big) - I_1^{\eta\eta} - I_2^{\eta\eta} - I_3^{\eta\eta}.\end{aligned} \tag{A.5}$$

Note that in Ref. [29] this extra term was not present in (5.21a), but correctly added in Ref. [20]. The other relaxation equations, together with $I_0$, $I_1^{\mu\nu}$, $I_2^{\mu\nu}$, and $I_3^{\mu\nu}$ and the vorticity tensor components remain formally unchanged.

(This is so, since all non-vanishing Christoffel symbols are multiplied with $u^\eta = 0$.)

## Appendix B: (3 + 1)-dimensional expansion in Cartesian coordinates

This case is very similar to the two-dimensional case discussed in Sect. 3.3. The only difference is that now the velocity, spatial derivative, and all four-vector and tensor components in the $z$ direction are non-zero. The velocity is $u^\mu = \gamma(1, v_x, v_y, v_z)$, where $\gamma = (1 - v_x^2 - v_y^2 - v_z^2)^{-1/2}$. Therefore, the new non-vanishing components of the charge four-current and energy momentum tensor, in addition to (94)–(96) and (97)–(102) which formally remain the same with $\gamma_\perp \to \gamma$, are

$$N^z \equiv N^0 v_z, \tag{B.1}$$

$$T^{0z} \equiv (e+P)\gamma^2 v_z + \pi^{0z}, \tag{B.2}$$

$$T^{zz} \equiv (e+P)\gamma^2 v_z^2 + P + \pi^{zz}, \tag{B.3}$$

$$T^{xz} \equiv (e+P)\gamma^2 v_x v_z + \pi^{xz}, \tag{B.4}$$

$$T^{yz} \equiv (e+P)\gamma^2 v_y v_z + \pi^{yz}. \tag{B.5}$$

The LRF quantities are calculated similarly to the (2 + 1)-dimensional case, thus

$$n = N^0\sqrt{1 - v_x^2 - v_y^2 - v_z^2}, \tag{B.6}$$

$$\begin{aligned} e = {} & \left(T^{00} - \pi^{00}\right) - v_x\left(T^{0x} - \pi^{0x}\right) \\ & - v_y\left(T^{0y} - \pi^{0y}\right) - v_z\left(T^{0z} - \pi^{0z}\right). \end{aligned} \tag{B.7}$$

While the velocity components in $x$ and $y$ directions remain the same as in Sect. 3.3, the velocity component in $z$ direction is

$$v_z = \frac{T^{0z} - \pi^{0z}}{T^{00} - \pi^{00} + P}. \tag{B.8}$$

The charge conservation equation is

$$\partial_t N^0 + \partial_x\left(v_x N^0\right) + \partial_y\left(v_y N^0\right) + \partial_z\left(v_z N^0\right) = 0. \tag{B.9}$$

The energy–momentum equations are

$$\begin{aligned} & \partial_t T^{00} + \partial_x\left(v_x T^{00}\right) + \partial_y\left(v_y T^{00}\right) + \partial_z\left(v_z T^{00}\right) \\ & \quad = -\partial_x\left(v_x P - v_x\pi^{00} + \pi^{0x}\right) - \partial_y\left(v_y P - v_y\pi^{00} + \pi^{0y}\right) \\ & \qquad - \partial_z\left(v_z P - v_z\pi^{00} + \pi^{0z}\right), \end{aligned} \tag{B.10}$$

$$\begin{aligned} & \partial_t T^{0x} + \partial_x\left(v_x T^{0x}\right) + \partial_y\left(v_y T^{0x}\right) + \partial_z\left(v_z T^{0x}\right) \\ & \quad = -\partial_x\left(P - v_x\pi^{0x} + \pi^{xx}\right) - \partial_y\left(-v_y\pi^{0x} + \pi^{xy}\right) \\ & \qquad - \partial_z\left(-v_z\pi^{0x} + \pi^{xz}\right), \end{aligned} \tag{B.11}$$

$$\begin{aligned} & \partial_t T^{0y} + \partial_x\left(v_x T^{0y}\right) + \partial_y\left(v_y T^{0y}\right) + \partial_z\left(v_z T^{0y}\right) \\ & \quad = -\partial_x\left(-v_x\pi^{0y} + \pi^{xy}\right) - \partial_y\left(P - v_y\pi^{0y} + \pi^{yy}\right) \\ & \qquad - \partial_z\left(-v_z\pi^{0y} + \pi^{yz}\right), \end{aligned} \tag{B.12}$$

$$\begin{aligned} & \partial_t T^{0z} + \partial_x\left(v_x T^{0z}\right) + \partial_y\left(v_y T^{0z}\right) + \partial_z\left(v_z T^{0z}\right) \\ & \quad = -\partial_x\left(-v_x\pi^{0z} + \pi^{xz}\right) - \partial_y\left(-v_y\pi^{0z} + \pi^{yz}\right) \\ & \qquad - \partial_z\left(P - v_z\pi^{0z} + \pi^{zz}\right). \end{aligned} \tag{B.13}$$

The relaxation equations are formally similar to (119), (120), only the $z$-directed derivatives $\gamma v_z \partial_z \Pi$ and $\gamma v_z \partial_z \pi^{\mu\nu}$ have to be added. Therefore, the new components of the shear tensor are

$$\begin{aligned} \sigma^{0z} = {} & \frac{1}{2}\left[\partial_t(\gamma v_z) - \partial_z\gamma\right] \\ & - \frac{1}{2}\left[\gamma D(\gamma v_z) + \gamma v_z D\gamma\right] + \gamma^2 v_z\frac{\theta}{3}, \end{aligned} \tag{B.14}$$

$$\sigma^{zz} = -\partial_z(\gamma v_z) - \gamma v_z D(\gamma v_z) + \left(1 + \gamma^2 v_z^2\right)\frac{\theta}{3}, \tag{B.15}$$

$$\begin{aligned} \sigma^{xz} = {} & -\frac{1}{2}\left[\partial_x(\gamma v_z) + \partial_z(\gamma v_x)\right] \\ & - \frac{1}{2}\left[\gamma v_x D(\gamma v_z) + \gamma v_z D(\gamma v_x)\right] + \gamma^2 v_x v_z\frac{\theta}{3}, \end{aligned} \tag{B.16}$$

$$\begin{aligned} \sigma^{yz} = {} & -\frac{1}{2}\left[\partial_y(\gamma v_z) + \partial_z(\gamma v_y)\right] \\ & - \frac{1}{2}\left[\gamma v_y D(\gamma v_z) + \gamma v_z D(\gamma v_y)\right] + \gamma^2 v_y v_z\frac{\theta}{3}, \end{aligned} \tag{B.17}$$

where the expansion scalar is $\theta = \partial_t\gamma + \partial_x(\gamma v_x) + \partial_y(\gamma v_y) + \partial_z(\gamma v_z)$, and the convective time derivative is $D \equiv u^\mu\partial_\mu = \gamma\partial_t + \gamma v_x\partial_x + \gamma v_y\partial_y + \gamma v_z\partial_z$. The form of the other components does not change in comparison with (121)–(126).

The term $I_1^{\mu\nu} = (\pi^{\lambda\mu}u^\nu + \pi^{\lambda\nu}u^\mu)Du_\lambda$ leads to

$$\begin{aligned} I_1^{00} = {} & 2\gamma\left[\pi^{00}D\gamma - \pi^{0x}D(\gamma v_x) - \pi^{0y}D(\gamma v_y)\right. \\ & \left. - \pi^{0z}D(\gamma v_z)\right], \end{aligned} \tag{B.18}$$

$$\begin{aligned} I_1^{0x} = {} & \gamma\left[\left(\pi^{00}v_x + \pi^{0x}\right)D\gamma - \left(\pi^{0x}v_x + \pi^{xx}\right)D(\gamma v_x)\right. \\ & - \left(\pi^{0y}v_x + \pi^{xy}\right)D(\gamma v_y) \\ & \left. - \left(\pi^{0z}v_x + \pi^{xz}\right)D(\gamma v_z)\right], \end{aligned} \tag{B.19}$$

$$\begin{aligned} I_1^{0y} = {} & \gamma\left[\left(\pi^{00}v_y + \pi^{0y}\right)D\gamma - \left(\pi^{0x}v_y + \pi^{xy}\right)D(\gamma v_x)\right. \\ & - \left(\pi^{0y}v_y + \pi^{yy}\right)D(\gamma v_y) \\ & \left. - \left(\pi^{0z}v_y + \pi^{yz}\right)D(\gamma v_z)\right], \end{aligned} \tag{B.20}$$

$$I_1^{0z} = \gamma\big[\big(\pi^{00}v_z + \pi^{0z}\big)D\gamma - \big(\pi^{0x}v_z + \pi^{xz}\big)D(\gamma v_x) - \big(\pi^{0y}v_z + \pi^{yz}\big)D(\gamma v_y) - \big(\pi^{0z}v_z + \pi^{zz}\big)D(\gamma v_z)\big], \tag{B.21}$$

$$I_1^{xx} = 2\gamma v_x\big[\pi^{0x}D\gamma - \pi^{xx}D(\gamma v_x) - \pi^{xy}D(\gamma v_y) - \pi^{xz}D(\gamma v_z)\big], \tag{B.22}$$

$$I_1^{yy} = 2\gamma v_y\big[\pi^{0y}D\gamma - \pi^{xy}D(\gamma v_x) - \pi^{yy}D(\gamma v_y) - \pi^{yz}D(\gamma v_z)\big], \tag{B.23}$$

$$I_1^{zz} = 2\gamma v_z\big[\pi^{0z}D\gamma - \pi^{xz}D(\gamma v_x) - \pi^{yz}D(\gamma v_y) - \pi^{zz}D(\gamma v_z)\big], \tag{B.24}$$

$$I_1^{xy} = \gamma\big[\big(\pi^{0x}v_y + \pi^{0y}v_x\big)D\gamma - \big(\pi^{xx}v_y + \pi^{xy}v_x\big)D(\gamma v_x) - \big(\pi^{xy}v_y + \pi^{yy}v_x\big)D(\gamma v_y) - \big(\pi^{xz}v_y + \pi^{yz}v_x\big)D(\gamma v_z)\big], \tag{B.25}$$

$$I_1^{xz} = \gamma\big[\big(\pi^{0x}v_z + \pi^{0z}v_x\big)D\gamma - \big(\pi^{xx}v_z + \pi^{xz}v_x\big)D(\gamma v_x) - \big(\pi^{xy}v_z + \pi^{yz}v_x\big)D(\gamma v_y) - \big(\pi^{xz}v_z + \pi^{zz}v_x\big)D(\gamma v_z)\big], \tag{B.26}$$

$$I_1^{yz} = \gamma\big[\big(\pi^{0y}v_z + \pi^{0z}v_y\big)D\gamma - \big(\pi^{xy}v_z + \pi^{xz}v_y\big)D(\gamma v_x) - \big(\pi^{yy}v_z + \pi^{yz}v_y\big)D(\gamma v_y) - \big(\pi^{yz}v_z + \pi^{zz}v_y\big)D(\gamma v_z)\big]. \tag{B.27}$$

The terms $I_0$ and $I_2^{\mu\nu}$ are given by (21) and (23). The new components which need to be computed compared to the previous case are $I_2^{0z}$, $I_2^{xz}$, $I_2^{yz}$, and $I_2^{zz}$. The non-vanishing components of the last term are

$$I_3^{00} = 2\big(\pi^{0x}\omega^0{}_x + \pi^{0y}\omega^0{}_y + \pi^{0z}\omega^0{}_z\big), \tag{B.28}$$

$$I_3^{0x} = \pi^{00}\omega^x{}_0 + \pi^{0y}\omega^x{}_y + \pi^{0z}\omega^x{}_z + \pi^{xx}\omega^0{}_x + \pi^{xy}\omega^0{}_y + \pi^{xz}\omega^0{}_z, \tag{B.29}$$

$$I_3^{0y} = \pi^{00}\omega^y{}_0 + \pi^{0x}\omega^y{}_x + \pi^{0z}\omega^y{}_z + \pi^{xy}\omega^0{}_x + \pi^{yy}\omega^0{}_y + \pi^{yz}\omega^0{}_z, \tag{B.30}$$

$$I_3^{0z} = \pi^{00}\omega^z{}_0 + \pi^{0x}\omega^z{}_x + \pi^{0y}\omega^z{}_y + \pi^{xz}\omega^0{}_x + \pi^{yz}\omega^0{}_y + \pi^{zz}\omega^0{}_z, \tag{B.31}$$

$$I_3^{xx} = 2\big(\pi^{0x}\omega^x{}_0 + \pi^{xy}\omega^x{}_y + \pi^{xz}\omega^x{}_z\big), \tag{B.32}$$

$$I_3^{yy} = 2\big(\pi^{0y}\omega^y{}_0 + \pi^{xy}\omega^y{}_x + \pi^{yz}\omega^y{}_z\big), \tag{B.33}$$

$$I_3^{zz} = 2\big(\pi^{0z}\omega^z{}_0 + \pi^{xz}\omega^z{}_x + \pi^{yz}\omega^z{}_y\big), \tag{B.34}$$

$$I_3^{xy} = \pi^{0x}\omega^y{}_0 + \pi^{xx}\omega^y{}_x + \pi^{xz}\omega^y{}_z + \pi^{0y}\omega^x{}_0 + \pi^{yy}\omega^x{}_y + \pi^{yz}\omega^x{}_z, \tag{B.35}$$

$$I_3^{xz} = \pi^{0x}\omega^z{}_0 + \pi^{xx}\omega^z{}_x + \pi^{xy}\omega^z{}_y + \pi^{0z}\omega^x{}_0 + \pi^{yz}\omega^x{}_y + \pi^{zz}\omega^x{}_z, \tag{B.36}$$

$$I_3^{yz} = \pi^{0y}\omega^z{}_0 + \pi^{xy}\omega^z{}_x + \pi^{yy}\omega^z{}_y + \pi^{0z}\omega^y{}_0 + \pi^{xz}\omega^y{}_x + \pi^{zz}\omega^y{}_z, \tag{B.37}$$

where the new vorticity tensor components are

$$\omega^0{}_z = \frac{1}{2}\big[\partial_z\gamma + \partial_t(\gamma v_z) + \gamma v_z D\gamma - \gamma D(\gamma v_z)\big], \tag{B.38}$$

$$\omega^x{}_z = \frac{1}{2}\big[\partial_z(\gamma v_x) - \partial_x(\gamma v_z)\big] + \frac{1}{2}\big[\gamma v_z D(\gamma v_x) - \gamma v_x D(\gamma v_z)\big], \tag{B.39}$$

$$\omega^y{}_z = \frac{1}{2}\big[\partial_z(\gamma v_y) - \partial_y(\gamma v_z)\big] + \frac{1}{2}\big[\gamma v_z D(\gamma v_y) - \gamma v_y D(\gamma v_z)\big], \tag{B.40}$$

such that $\omega^0{}_z = \omega^z{}_0 = -\omega^{0z} = \omega_{0z}$, $\omega^x{}_z = -\omega^z{}_x = -\omega^{xz} = -\omega_{xz}$ and $\omega^y{}_z = -\omega^z{}_y = -\omega^{yz} = -\omega_{yz}$. The other components are given in (140)–(142) where one has to replace $\gamma_\perp$ with $\gamma$.

## Appendix C: (3 + 1)-dimensional expansion in $(\tau, x, y, \eta)$ coordinates

The metric of the space-time is the same as in Appendix A, only the definition of the flow velocity changes. In this case the contravariant flow velocity is $u^\mu = \gamma(1, v_x, v_y, v_\eta)$, and the covariant flow velocity is $u_\mu = g_{\mu\nu}u^\nu = \gamma(1, -v_x, -v_y, -\tau^2 v_\eta)$, where $\gamma = (1 - v_x^2 - v_y^2 - \tau^2 v_\eta^2)^{-1/2}$. The gradients are, $\partial_\mu = (\partial_\tau, \partial_x, \partial_y, \partial_\eta)$ and $\partial^\mu \equiv g^{\mu\nu}\partial_\nu = (\partial_\tau, -\partial_x, -\partial_y, -\tau^{-2}\partial_\eta)$.

Similarly as before the equations can be easily obtained from the ones found in Cartesian coordinates in Appendix B. All laboratory frame quantities are formally the same, except for $T^{zz} \to T^{\eta\eta} \equiv (e+P)\gamma^2 v_\eta^2 + P/\tau^2 + \pi^{\eta\eta}$. The LRF quantities are

$$n = N^0\sqrt{1 - v_x^2 - v_y^2 - \tau^2 v_\eta^2}, \tag{C.1}$$

$$e = \big(T^{00} - \pi^{00}\big) - v_x\big(T^{0x} - \pi^{0x}\big) - v_y\big(T^{0y} - \pi^{0y}\big) - \tau^2 v_\eta\big(T^{0\eta} - \pi^{0\eta}\big). \tag{C.2}$$

The velocity components $v_x$ and $v_y$ are given by (106), (107), the velocity component in $\eta$-direction is given similarly as in (B.8). The charge conservation equation is given by

$$\partial_\tau N^\tau + \partial_x\big(v_x N^\tau\big) + \partial_y\big(v_y N^\tau\big) + \partial_\eta\big(v_\eta N^\tau\big) = -\frac{1}{\tau}N^\tau. \tag{C.3}$$

The equation for energy–momentum conservation leads to

$$\begin{aligned}\partial_\tau T^{\tau\tau} &+ \partial_x\big(v_x T^{\tau\tau}\big) + \partial_y\big(v_y T^{\tau\tau}\big) + \partial_\eta\big(v_\eta T^{\tau\tau}\big)\\ &= -\partial_x\big(v_x P - v_x\pi^{\tau\tau} + \pi^{\tau x}\big) - \partial_y\big(v_y P - v_y\pi^{\tau\tau} + \pi^{\tau y}\big)\\ &\quad - \partial_\eta\big(v_\eta P - v_\eta\pi^{\tau\tau} + \pi^{\tau\eta}\big) - \frac{1}{\tau}\big(T^{\tau\tau} + \tau^2 T^{\eta\eta}\big),\end{aligned} \tag{C.4}$$

$$\begin{aligned}\partial_\tau T^{\tau x} &+ \partial_x\big(v_x T^{\tau x}\big) + \partial_y\big(v_y T^{\tau x}\big) + \partial_\eta\big(v_\eta T^{\tau x}\big)\\ &= -\partial_x\big(P - v_x\pi^{\tau x} + \pi^{xx}\big) - \partial_y\big(-v_y\pi^{\tau x} + \pi^{xy}\big)\\ &\quad - \partial_y\big(-v_\eta\pi^{\tau x} + \pi^{x\eta}\big) - \frac{1}{\tau}T^{\tau x},\end{aligned} \tag{C.5}$$

$$\begin{aligned}\partial_\tau T^{\tau y} &+ \partial_x\big(v_x T^{\tau y}\big) + \partial_y\big(v_y T^{\tau y}\big) + \partial_\eta\big(v_\eta T^{\tau y}\big)\\ &= -\partial_x\big(-v_x\pi^{\tau y} + \pi^{xy}\big) - \partial_y\big(P - v_y\pi^{\tau y} + \pi^{yy}\big)\\ &\quad - \partial_\eta\big(-v_\eta\pi^{\tau y} + \pi^{y\eta}\big) - \frac{1}{\tau}T^{\tau y},\end{aligned} \tag{C.6}$$

$$\begin{aligned}\partial_\tau T^{\tau\eta} &+ \partial_x\big(v_x T^{\tau\eta}\big) + \partial_y\big(v_y T^{\tau\eta}\big) + \partial_\eta\big(v_\eta T^{\tau\eta}\big)\\ &= -\partial_x\big(-v_x\pi^{\tau\eta} + \pi^{x\eta}\big) - \partial_y\big(-v_y\pi^{\tau\eta} + \pi^{y\eta}\big)\\ &\quad - \partial_\eta\left(\frac{P}{\tau^2} - v_\eta\pi^{\tau\eta} + \pi^{\eta\eta}\right) - \frac{3}{\tau}T^{\tau\eta}.\end{aligned} \tag{C.7}$$

The relaxation equations for the bulk viscous pressure and the shear stress tensor components $\pi^{xx}, \pi^{yy}, \pi^{xy}$ are formally the same as in Cartesian coordinates, however, for the other components we obtain

$$D\pi^{\tau\tau} = -2\tau\gamma v_\eta\pi^{\tau\eta} + I^{\tau\tau}, \tag{C.8}$$

$$D\pi^{\tau x} = -\tau\gamma v_\eta\pi^{x\eta} + I^{\tau x}, \tag{C.9}$$

$$D\pi^{\tau y} = -\tau\gamma v_\eta\pi^{y\eta} + I^{\tau y}, \tag{C.10}$$

$$D\pi^{\tau\eta} = -\tau\gamma v_\eta\pi^{\eta\eta} - \frac{\gamma}{\tau}\pi^{\tau\eta} - \frac{\gamma v_\eta}{\tau}\pi^{\tau\tau} + I^{\tau\eta}, \tag{C.11}$$

$$D\pi^{x\eta} = -\frac{\gamma}{\tau}\pi^{x\eta} - \frac{\gamma v_\eta}{\tau}\pi^{\tau x} + I^{x\eta}, \tag{C.12}$$

$$D\pi^{y\eta} = -\frac{\gamma}{\tau}\pi^{y\eta} - \frac{\gamma v_\eta}{\tau}\pi^{\tau y} + I^{y\eta}, \tag{C.13}$$

$$D\pi^{\eta\eta} = -2\frac{\gamma}{\tau}\pi^{\eta\eta} - 2\frac{\gamma v_\eta}{\tau}\pi^{\tau\eta} + I^{\eta\eta}, \tag{C.14}$$

where $I^{\mu\nu}$ denotes the right-hand side of (18), but in this case $D = \gamma\partial_\tau + \gamma v_x\partial_x + \gamma v_y\partial_y + \gamma v_\eta\partial_\eta$ denotes the convective time derivative of scalars.

The shear tensor components $\sigma^{xx}, \sigma^{yy}$, and $\sigma^{xy}$ remain formally unchanged from (124), (125), (126), while the ones which are different are calculated from (9),

$$\sigma^{\tau\tau} = -\tau\gamma^3 v_\eta^2 + \partial_\tau\gamma - \gamma D\gamma + \big(\gamma^2 - 1\big)\frac{\theta}{3}, \tag{C.15}$$

$$\begin{aligned}\sigma^{\tau x} &= -\frac{\tau\gamma^3 v_\eta^2 v_x}{2} + \frac{1}{2}\big[\partial_\tau(\gamma v_x) - \partial_x\gamma\big]\\ &\quad - \frac{1}{2}\big[\gamma D(\gamma v_x) + \gamma v_x D\gamma\big] + \gamma^2 v_x\frac{\theta}{3},\end{aligned} \tag{C.16}$$

$$\begin{aligned}\sigma^{\tau y} &= -\frac{\tau\gamma^3 v_\eta^2 v_y}{2} + \frac{1}{2}\big[\partial_\tau(\gamma v_y) - \partial_y\gamma\big]\\ &\quad - \frac{1}{2}\big[\gamma D(\gamma v_y) + \gamma v_y D\gamma\big] + \gamma^2 v_y\frac{\theta}{3},\end{aligned} \tag{C.17}$$

$$\begin{aligned}\sigma^{\tau\eta} &= -\frac{\gamma^3 v_\eta}{2\tau}\big(2 + \tau^2 v_\eta^2\big) + \frac{1}{2}\left[\partial_\tau(\gamma v_\eta) - \frac{1}{\tau^2}\partial_\eta\gamma\right]\\ &\quad - \frac{1}{2}\big[\gamma D(\gamma v_\eta) + \gamma v_\eta D\gamma\big] + \gamma^2 v_\eta\frac{\theta}{3},\end{aligned} \tag{C.18}$$

$$\begin{aligned}\sigma^{\eta\eta} &= -\frac{\gamma}{\tau^3}\big(1 + 2\gamma^2 v_\eta^2\tau^2\big) - \frac{1}{\tau^2}\partial_\eta(\gamma v_\eta)\\ &\quad - \gamma v_\eta D(\gamma v_\eta) + \left(\frac{1}{\tau^2} + \gamma^2 v_\eta^2\right)\frac{\theta}{3},\end{aligned} \tag{C.19}$$

$$\begin{aligned}\sigma^{x\eta} &= -\frac{\gamma^3 v_x v_\eta}{\tau} - \frac{1}{2}\left[\partial_x(\gamma v_\eta) + \frac{1}{\tau^2}\partial_\eta(\gamma v_x)\right]\\ &\quad - \frac{1}{2}\big[\gamma v_x D(\gamma v_\eta) + \gamma v_\eta D(\gamma v_x)\big] + \gamma^2 v_x v_\eta\frac{\theta}{3},\end{aligned} \tag{C.20}$$

$$\begin{aligned}\sigma^{y\eta} &= -\frac{\gamma^3 v_y v_\eta}{\tau} - \frac{1}{2}\left[\partial_y(\gamma v_\eta) + \frac{1}{\tau^2}\partial_\eta(\gamma v_y)\right]\\ &\quad - \frac{1}{2}\big[\gamma v_y D(\gamma v_\eta) + \gamma v_\eta D(\gamma v_y)\big] + \gamma^2 v_y v_\eta\frac{\theta}{3},\end{aligned} \tag{C.21}$$

where the expansion scalar is $\theta = \gamma/\tau + \partial_t\gamma + \partial_x(\gamma v_x) + \partial_y(\gamma v_y) + \partial_\eta(\gamma v_\eta)$. The $I_0$, $I_1^{\mu\nu}$, $I_2^{\mu\nu}$, and $I_3^{\mu\nu}$ components remain formally the same. The new vorticity tensor components are

$$\begin{aligned}\omega^\tau{}_\eta &= \frac{1}{2}\big[\partial_\eta\gamma + \partial_\tau\big(\tau^2\gamma v_\eta\big)\big]\\ &\quad + \frac{1}{2}\big[\tau^2\gamma v_\eta D\gamma - \gamma D\big(\tau^2\gamma v_\eta\big)\big],\end{aligned} \tag{C.22}$$

$$\begin{aligned}\omega^x{}_\eta &= \frac{1}{2}\big[\partial_\eta(\gamma v_x) - \partial_x\big(\tau^2\gamma v_\eta\big)\big]\\ &\quad + \frac{1}{2}\big[\tau^2\gamma v_\eta D(\gamma v_x) - \gamma v_x D\big(\tau^2\gamma v_\eta\big)\big],\end{aligned} \tag{C.23}$$

$$\begin{aligned}\omega^y{}_\eta &= \frac{1}{2}\big[\partial_\eta(\gamma v_y) - \partial_y\big(\tau^2\gamma v_\eta\big)\big]\\ &\quad + \frac{1}{2}\big[\tau^2\gamma v_\eta D(\gamma v_y) - \gamma v_y D\big(\tau^2\gamma v_\eta\big)\big],\end{aligned} \tag{C.24}$$

where $\omega^\tau{}_\eta = \omega^\eta{}_\tau$, $\omega^x{}_\eta = -\omega^\eta{}_x$ and $\omega^y{}_\eta = -\omega^\eta{}_y$.

## References


1. S.Z. Belenkij, L.D. Landau, Nuovo Cim. Suppl. **3S10**, 15 (1956) [Usp. Fiz. Nauk 56, 309 (1955)]
2. RHIC Scientists Serve Up "Perfect" Liquid, http://www.bnl.gov/bnlweb/pubaf/pr/PR_display.asp?prID=05-38
3. P. Danielewicz, M. Gyulassy, Phys. Rev. D **31**, 53 (1985)
4. P. Kovtun, D.T. Son, A.O. Starinets, Phys. Rev. Lett. **94**, 111601 (2005). arXiv:hep-th/0405231
5. J.M. Stewart, *Lecture Notes in Physics*, vol. 10 (Springer, Berlin, 1971)
6. W. Israel, Ann. Phys. **100**, 310 (1976)
7. J.M. Stewart, Proc. R. Soc. A **357**, 59 (1977)
8. W. Israel, J.M. Stewart, Ann. Phys. **118**, 341 (1979)
9. I. Müller, Z. Phys. **198**, 329 (1967)
10. I. Müller, Living Rev. Relativ. **2**, 1 (1999). http://www.livingreviews.org/lrr-1999-1
11. A. Muronga, Phys. Rev. Lett. **88**, 062302 (2002). arXiv:nucl-th/0104064 [Erratum-ibid. **89**, 159901 (2002)]
12. A. Muronga, Phys. Rev. C **69**, 034903 (2004). arXiv:nucl-th/0309055
13. R. Baier, P. Romatschke, U.A. Wiedemann, Phys. Rev. C **73**, 064903 (2006). arXiv:hep-ph/0602249
14. R. Baier, P. Romatschke, Eur. Phys. J. C **51**, 677 (2007). arXiv:nucl-th/0610108
15. A. Dumitru, E. Molnar, Y. Nara, Phys. Rev. C **76**, 024910 (2007). arXiv:0706.2203 [nucl-th]
16. P. Huovinen, D. Molnar, Phys. Rev. C **79**, 014906 (2009). arXiv:0808.0953 [nucl-th]
17. A. Muronga, D.H. Rischke, arXiv:nucl-th/0407114
18. A.K. Chaudhuri, arXiv:0704.0134 [nucl-th]
19. P. Romatschke, U. Romatschke, Phys. Rev. Lett. **99**, 172301 (2007). arXiv:0706.1522 [nucl-th]
20. H. Song, U.W. Heinz, Phys. Lett. B **658**, 279 (2008). arXiv:0709.0742 [nucl-th]
21. H. Song, U.W. Heinz, Phys. Rev. C **77**, 064901 (2008). arXiv:0712.3715 [nucl-th]
22. A.K. Chaudhuri, arXiv:0801.3180 [nucl-th]
23. M. Luzum, P. Romatschke, Phys. Rev. C **78**, 034915 (2008). arXiv:0804.4015 [nucl-th] [Erratum-ibid. C **79** (2009) 039903]
24. H. Song, U.W. Heinz, Phys. Rev. C **78**, 024902 (2008). arXiv:0805.1756 [nucl-th]
25. C. Eckart, Phys. Rev. **58**, 919 (1940)
26. L.D. Landau, E.M. Lifshitz, *Fluid Dynamics*, 2nd edn. (Butterworth-Heinemann, London, 1987)
27. S.R. de Groot, W.A. van Leeuwen, Ch.G. van Weert, *Relativistic Kinetic Theory—Principles and Applications* (North-Holland, Amsterdam, 1980)
28. L.P. Csernai, *Introduction to Relativistic Heavy Ion Collisions* (Wiley, Amsterdam, 1994)
29. U.W. Heinz, H. Song, A.K. Chaudhuri, Phys. Rev. C **73**, 034904 (2006). arXiv:nucl-th/0510014
30. A. Muronga, Phys. Rev. C **76**, 014910 (2007). arXiv:nucl-th/0611091
31. A. Muronga, Phys. Rev. C **76**, 014909 (2007). arXiv:nucl-th/0611090
32. E. Molnar, Eur. Phys. J. C **60**, 413 (2009)
33. J.P. Boris, D.L. Book, J. Comput. Phys. **11**, 38 (1973)
34. J.P. Boris, NRL Memorandum Report, 3237, 1976
35. J.P. Boris, A.M. Landsberg, E.S. Oran, J.H. Gardner, NRL Memorandum Report 93-7192, 1993. http://www.lcp.nrl.navy.mil/lcpfct/
36. G. Tóth, D. Odstrcil, J. Comput. Phys. **128**, 82 (1996)
37. J. Liu, E.S. Oran, C.R. Kaplan, J. Comput. Phys. **208**, 416 (2005)
38. D.L. Book, C. Li, G. Patnaik, F.F. Grinstein, J. Sci. Comput. **6**, 323 (1991)
39. D.L. Book, J.P. Boris, K. Hain, J. Comput. Phys. **18**, 248 (1975)
40. C.R. DeVore, J. Comput. Phys. **92**, 142 (1991)
41. S.T. Zalesak, J. Comput. Phys. **31**, 335 (1979)
42. J.M. Marti, E. Mueller, Numerical Hydrodynamics in Special Relativity. arXiv:astro-ph/9906333
43. J.M. Marti, E. Mueller, Living Rev. Relativ. **6**, 7 (2003). http://www.livingreviews.org/lrr-2003-7
44. V. Schneider et al., J. Comput. Phys. **105**, 92 (1993)
45. D.H. Rischke, S. Bernard, J.A. Maruhn, Nucl. Phys. A **595**, 346 (1995)
46. D.H. Rischke, arXiv:nucl-th/9809044
47. J.J. Monaghan, Comput. Phys. Commun. **48**, 88 (1988)
48. J.J. Monaghan, Rep. Prog. Phys. **68**, 1703 (2005)
49. P. Mota, G.S. Denicol, T. Kodama, Braz. J. Phys. **37**, 671 (2007)
50. G.S. Denicol, T. Kodama, T. Koide, P. Mota, Phys. Rev. C **78**, 034901 (2008). arXiv:0805.1719 [hep-ph]
51. G.S. Denicol, T. Kodama, T. Koide, P. Mota, J. Phys. G **36**, 035103 (2009)
52. G.S. Denicol, T. Kodama, T. Koide, P. Mota, arXiv:0903.3595 [hep-ph]
53. F.H. Harlow, Proc. Symp. Appl. Math. **15**, 269 (1963)
54. F.H. Harlow, Methods Comput. Phys. **3**, 319 (1964)
55. J.A. Font, Living Rev. Relativ. **11**, 7 (2008). http://www.livingreviews.org/lrr-2008-7
56. P.D. Lax, Appl. Math. **7**, 159 (1954)
57. H. Nessyahu, E. Tadmor, J. Comput. Phys. **87**, 408 (1990)
58. A. Kurganov, E. Tadmor, J. Comput. Phys. **160**, 214 (2000)
59. http://www.cscamm.umd.edu/centpack/index.htm
60. A. Lucas-Serrano, J.A. Font, J.M. Ibanez, J.M. Marti, Astron. Astrophys. **428**, 703 (2004). arXiv:astro-ph/0407541
61. L. Pareschi, SIAM J. Numer. Anal. **39**(4), 1395 (2001)
62. M. Grmela, H.C. Ottinger, Phys. Rev. E **56**, 6620 (1997)
63. K. Dusling, D. Teaney, Phys. Rev. C **77**, 034905 (2008). arXiv:0710.5932 [nucl-th]
64. Z. Xu, C. Greiner, Phys. Rev. C **71**, 064901 (2005). arXiv:hep-ph/0406278
65. I. Bouras, A. El, O. Fochler, C. Greiner, E. Molnar, H. Niemi, Z. Xu, Acta Phys. Pol. B **40**, 973 (2009)
66. I. Bouras, E. Molnar, H. Niemi, Z. Xu, A. El, O. Fochler, C. Greiner, D.H. Rischke, Phys. Rev. Lett. **103**, 032301 (2009). arXiv:0902.1927 [hep-ph]
67. I. Bouras et al., in preparation